

# Neon and CNO Abundances for Extreme Helium Stars – A Non-LTE Analysis

Gajendra Pandey

*Indian Institute of Astrophysics; Bangalore, 560034 India*

pandey@iiap.res.in

and

David L. Lambert

*The W.J. McDonald Observatory, University of Texas at Austin; Austin, TX 78712-1083*

dll@astro.as.utexas.edu

## ABSTRACT

A non-LTE (NLTE) abundance analysis was carried out for three extreme helium stars (EHes): BD+10° 2179, BD−9° 4395, and LSIV +6° 002, from their optical spectra with NLTE model atmospheres. NLTE TLUSTY model atmospheres were computed with H, He, C, N, O, and Ne treated in NLTE. Model atmosphere parameters were chosen from consideration of fits to observed He I line profiles and ionization equilibria of C and N ions. The program SYNSPEC was then used to determine the NLTE abundances for Ne as well as H, He, C, N, and O. LTE neon abundances from Ne I lines in the EHes: LSE 78, V1920 Cyg, HD 124448, and PV Tel, are derived from published models and an estimate of the NLTE correction applied to obtain the NLTE Ne abundance.

We show that the derived abundances of these key elements, including Ne, are well matched with semi-quantitative predictions for the EHe resulting from a cold merger (i.e., no nucleosynthesis during the merger) of a He white dwarf with a C-O white dwarf.

*Subject headings:* stars: atmospheres – stars: fundamental parameters – stars: abundances – stars: chemically peculiar – stars: evolution

## 1. Introduction

The principal class of hydrogen-deficient supergiant stars comprises three subclasses which in order of increasing but overlapping temperature intervals from coolest to hottest are the H-deficient carbon stars (HdC), the R Coronae Borealis stars (RCB), and the extreme helium stars (EHe). A common supposition is that the three subclasses are related in terms of origin and evolution. The origin of these very rare stars has long been disputed but it now seems likely that the majority are formed through a merger of a He white dwarf with a C-O white dwarf, the so-called double degenerate (DD) scenario (Webbink 1984; Iben & Tutukov 1984; Saio & Jeffery 2002). Others may be the result of a final He-shell flash in a post-AGB star, the so-called final flash (FF) scenario (Iben et al. 1983; Iben, Tutukov & Yungelson 1996; Herwig 2001; Blöcker 2001).

Much of the evidence for deciding whether HdC, RCB, or EHe stars come from the DD or FF scenario (or neither) depends on comparison of the observed chemical composition with predictions by the two scenarios. It is in this context that we present in this paper a non-LTE (NLTE) analysis of the neon abundance of a sample of EHe stars where Ne I lines are prominent in optical spectra; neon is detectable in EHe stars, the warmer RCBs but not the HdCs. (The NLTE analyses are extended here to He, C, N, and O lines.)

If reliable Ne abundances can be provided for EHes and RCBs, neon will join other abundances as clues to the origins and evolution of the H-deficient supergiants. In addition to the obvious importance of C, N, and O elemental abundances, one may now note a variety of other abundance anomalies peculiar to these supergiants including, for example, the presence of lithium in a subset of RCBs and one HdC (Asplund et al. 2000; Rao & Lambert 1996), the large overabundance of fluorine in EHes and RCBs (Pandey 2006; Pandey, Lambert & Rao 2008), high concentrations of  $^{18}\text{O}$  (relative to  $^{16}\text{O}$ ) in HdCs and cool RCBs (Clayton et al. 2005, 2007; García-Hernández et al. 2009, 2010), extraordinary high Si/Fe and S/Fe ratios in the ‘minority’ RCBs (Rao & Lambert 1996).

If neon is to provide an effective addition to the list of abundance anomalies, its abundance must be determined reliably and, in this regard, the primary consideration would appear to be an adequate treatment of NLTE effects in the formation of the observable neon lines. Realization that NLTE effects are considerable for optical Ne I lines arose from pioneering calculations by Auer & Mihalas (1973) for normal B-type stars with effective temperatures of around 20,000 K. These authors showed that the Ne abundance derived by accounting for NLTE effects was about a factor of five less than that given by LTE. Not only was this the first result showing major NLTE effects on abundances for hot stars but the NLTE Ne abundance was shown to be in good agreement with that for H II regions as derived from emission lines. The origin of the marked NLTE effects is discussed by Auer

& Mihalas. A key ingredient is that the ultraviolet Ne I resonance lines are optically thick — see a concise discussion by Cunha, Hubeny & Lanz (2006) who report on modern calculations of Ne NLTE effects as applied to B stars in the Orion Association. Given that the ultraviolet resonance lines may be similarly optically thick in atmospheres of EHe stars, it became apparent that addition of neon to the list of referees between DD and FF scenarios would require evaluation of the NLTE effects on the observable neon lines.

In the following sections, we successively describe our optical spectra, the NLTE calculations including a sanity check involving our analysis of normal B stars previously discussed by Cunha, Hubeny & Lanz (2006) and Morel & Butler (2008), our abundance analyses of seven EHes, a discussion of the DD scenario with a comparison of semi-quantitative predictions with the observationally-based abundances of He, C, O, and Ne as well as remarks on abundances not determinable for EHes (e.g., Li,  $^{18}\text{O}$ , and F). This comparison is followed by remarks on the FF scenario and a few concluding remarks.

## 2. Observations

High-resolution optical spectra of BD+10° 2179, BD−9° 4395 and V1920 Cyg were obtained on 24 January 1998, 16 June 2000, and 25 July 1996, respectively, at the coudé focus of the W.J. McDonald Observatory’s Harlan J. Smith 2.7-m telescope with the Robert G. Tull cross-dispersed echelle spectrograph (Tull et al. 1995) at a resolving power of  $R=60,000$  except for BD−9° 4395’s spectrum acquired at  $R=40,000$ . These spectra with  $R=60,000$  were previously described by Pandey et al. (2006). Additional spectra of BD−9° 4395 were obtained on 18, 22, and 25 July 2002 at the W.J. McDonald Observatory’s Otto Struve 2.1-m telescope with the Sandiford Caasegrain echelle spectrograph (McCarthy et al. 1993) at a resolving power of  $R=40,000$ . The spectrum of LSE 78 was acquired with the Cassegrain echelle spectrograph at CTIO, and the observations are described in Pandey & Reddy (2006). Finally, spectra at  $R=30,000$  of the two southern EHes – PV Tel and HD 124448 – are from the Vainu Bappu Observatory and the fiber-fed cross-dispersed echelle spectrometer (Rao et al. 2004, 2005) at the 2.34-m telescope. The Image Reduction and Analysis Facility (IRAF) software package was used to reduce all spectra.<sup>1</sup>

Sample wavelength intervals in Figures 1 and 2 include one or two of the Ne I lines with the EHes ordered from top to bottom in order of decreasing effective temperature. All spectra are aligned to the rest wavelengths of well-known lines. Inspection of the figures

---

<sup>1</sup>The IRAF software is distributed by the National Optical Astronomy Observatories under contract with the National Science Foundation

shows that the line profiles are not always symmetric. Asymmetries obviously present in the case of LSE 78 and V1920 Cyg are most probably due to atmospheric pulsations. In the case of V1920 Cyg, another observation on 1996 July 26, one day following the spectrum illustrated in Figures 1 and 2, showed symmetric line profiles with no appreciable change in the equivalent widths of lines. The equivalent width change translates to an abundance change of less than 0.1 dex. In the case of BD–9° 4395, emission components may appear and disappear. Variable photospheric spectra for EHes are common (Jeffery 2008) with V1920 Cyg representative of the variability and BD–9° 4395 as an extreme example. Nonetheless, we assume that models constructed with classical assumptions (plane parallel layers in hydrostatic equilibrium) are adequate for our purpose.

### 3. NLTE Atmospheres and Abundances

Our calculations use codes developed by Hubeny and colleagues, that is the program TLUSTY for calculating LTE and NLTE model atmospheres (Hubeny 1988; Hubeny & Lanz 1995) and the spectrum synthesis code SYNSPEC (Hubeny, Lanz & Jeffery 1995). In exercising these codes, we adopt the atomic data and model atoms provided on the TLUSTY homepage<sup>2</sup> (Lanz & Hubeny 2007, 2003).

The suite of codes was imported to Bangalore and run by one of us (GP) on a local computer. Before proceeding to construct and apply H-deficient model atmospheres, our imported codes were tested for normal B-type stars. In particular, we computed a NLTE model atmosphere for HD 35299, a normal B star in the Orion sample for which Cunha, Hubeny & Lanz (2006) derived NLTE Ne abundances. The NLTE TLUSTY model was computed for the stellar parameters adopted by Cunha et al.:  $T_{\text{eff}} = 24000\text{K}$ ,  $\log g = 4.25$  cgs and a microturbulence of  $2 \text{ km s}^{-1}$  and solar abundances. The  $gf$ -values for the Ne I lines are taken from Seaton (1998) who showed that Opacity Project theoretical  $gf$ -values are in very good agreement not only with theoretical calculations of comparable sophistication but also with experimental determinations. Then, the NLTE Ne abundances were computed using the TLUSTY model by matching the observed equivalent width of Ne I lines with NLTE predictions from running the SYNSPEC code. Observed equivalent widths were kindly provided by Dr. Katia Cunha (private communication) for the eight lines measured by them. Our NLTE Ne abundance for the eight lines is  $\log(\text{Ne}) = 8.20 \pm 0.08$  in good agreement with the value of 8.18 given by Cunha et al. This agreement over NLTE Ne abundances is taken as evidence that our implementation of the TLUSTY-related codes was successful.

---

<sup>2</sup><http://nova.astro.umd.edu/index.html>

As a second check, we analysed Ne I and Ne II lines in  $\beta$  CMa. Morel & Butler (2008) analyzed 7 Ne I and 4 Ne II lines in this star. Morel & Butler compute the NLTE Ne abundances for a LTE Kurucz model with the parameters:  $T_{\text{eff}} = 24000\text{K}$ ,  $\log g = 3.5$  cgs and a microturbulence of  $14 \text{ km s}^{-1}$ . We computed a NLTE TLUSTY model for these stellar parameters. The  $gf$ -values and the measured equivalent widths of the Ne I and the Ne II lines were taken from Morel & Butler. NLTE Ne abundances were computed using the TLUSTY atmosphere and model atoms by matching the measured width of Ne I and Ne II lines with NLTE predictions from the SYNSPEC code. Our NLTE Ne abundance for the seven Ne I lines is  $\log(\text{Ne}) = 7.89 \pm 0.09$  in agreement with the value of  $7.89 \pm 0.04$  given by Morel & Butler. For the three Ne II lines, our NLTE Ne abundance is  $\log(\text{Ne}) = 8.16 \pm 0.16$  where the value of  $7.89 \pm 0.06$  is given by Morel & Butler. Note that, one of the four Ne II lines returns a higher abundance and was not included in calculating our mean abundance. The different Ne abundances from Ne II lines is noted and may arise from the use of different models (TLUSTY NLTE versus Kurucz LTE) and the use of different model Ne atoms. These checks on published NLTE Ne abundances are taken as evidence that our implementation of the TLUSTY-related codes was successful.

A small grid of NLTE TLUSTY model atmospheres for EHe stars was computed for  $T_{\text{eff}}$  from 15,000 K to 31,000 K and surface gravities  $\log g = 2.35$  to 4.3. The abundances adopted for the grid were representative of the LTE abundances given by Pandey et al. (2006). In particular, the C/He ratio was assumed to be 1 per cent. Sample models for H/He=0.1 and 0.0001 showed that the derived abundances of neon and other elements are insensitive to the H abundance in this range.

## 4. NLTE Abundance Analyses

### 4.1. BD +10° 2179

An extensive LTE abundance analysis of BD+10° 2179 was reported by Pandey et al. (2006) from optical and ultraviolet spectra. Abundances were obtained for 18 elements from H to Zn but neon was not included. Here, we present a NLTE model atmosphere redetermination of the He, C, N, and O abundances and the first determination of the Ne abundance. The star’s atmospheric parameters are reassessed using NLTE atmospheres and NLTE line formation for He, C, N, O and Ne lines.

Optical lines of He I, C I-III, N II, O II and Ne I are used. Details about these lines except for Ne I are taken from Table 2 of (Pandey et al. 2006). Details include a line’s  $gf$ -value and the reference to the source of that value, its lower excitation potential ( $\chi$ ), and information

on the line’s Stark and radiative damping constants. Values from 2006 are adopted here in full. For Ne which is not in the 2006 Table, we adopt the  $gf$ -values from Seaton (1998), as noted above. Table 1 of this paper lists the chosen lines of C, N, O, and Ne where the equivalent widths of Ne I lines were measured off the spectrum used for the 2006 analysis.

Atmospheric parameters are obtained by the procedures used for the 2006 LTE analysis but using NLTE TLUSTY model atmospheres and NLTE line formation using the TLUSTY model atoms. The microturbulence is provided from the usual requirement that the abundance from lines of a given species be independent of a line’s equivalent width: we use the C II lines. The effective temperature and surface gravity are found from intersecting loci in the ( $T_{\text{eff}}$ ,  $\log g$ ) plane with loci provided by fits to He I line profiles, and the ionization equilibria among C<sup>o</sup>, C<sup>+</sup>, and C<sup>2+</sup>. The LTE analysis is repeated but this time with TLUSTY LTE model atmospheres instead of models from the code STERNE (Jeffery, Woolf & Pollacco 2001).

Figure 3 illustrates the determination of the microturbulence from C II lines. A value of 7.5 km s<sup>-1</sup> is adopted. Although this value is for a particular model ( $T_{\text{eff}}=17000\text{K}$ ,  $\log g=2.5$ ), the result is insensitive to the model choice.

Sample theoretical NLTE line profiles and the observed profile of the He I 4471Å line are shown in Figure 4 for a model with an effective temperature of 16,375K and a surface gravity of 2.45 g cm<sup>-2</sup> and with microturbulence and rotational broadening included (see Pandey et al. (2006)). The best-fitting theoretical profile ( $\log g=2.45$ ) provides one point on the  $T_{\text{eff}} - \log g$  locus. The He I lines at 4009, 4026, and 4387 Å lines were similarly analysed. The helium model atoms and line broadening coefficients are from TLUSTY. Using the TLUSTY grid of model atmospheres, the loci were mapped out. The four loci are shown in Figure 5 and are almost coincident.

Loci representing ionization equilibrium are provided from the requirements that (C I, C II), (C II, C III), and (C I, C III) provide the same C abundance.

Figure 5 shows the several loci. Their intersection suggests that the best NLTE model has  $T_{\text{eff}}=16375\pm 250\text{K}$  and  $\log g = 2.45\pm 0.2$ . The best LTE TLUSTY model with the LTE line analysis gives a best model with  $T_{\text{eff}} = 17000\text{K}$  and  $\log g=2.60$ . This LTE model differs a little from that adopted in the 2006 LTE analysis of the optical lines where loci representing ionization equilibria for (Si II, Si III), (S II, S III), and (Fe II, Fe III) were also considered. The 2006 LTE analysis gave a model with  $T_{\text{eff}}=16400\pm 500\text{K}$  and  $\log g=2.35\pm 0.2$  cgs.

Abundances for C, N, O, and Ne are given in Table 1. Mean abundances and their standard deviations are listed for both the NLTE and LTE TLUSTY analyses. Abundances are given as  $\log \epsilon(X)$  and normalized to  $\log \sum \mu_X \epsilon(X) = 12.15$  where  $\mu_X$  is the atomic weight of element X. The NLTE abundance errors arising from uncertainties in the atmospheric

parameters are estimated by considering changes of  $\Delta T = \pm 250\text{K}$ ,  $\Delta \log g = \pm 0.2$  cgs, and  $\Delta \xi = \pm 1 \text{ km s}^{-1}$ . The rms errors in the abundances from C I, C II, C III, N II, O II, and Ne I are 0.22, 0.03, 0.18, 0.08, 0.12, and 0.10, respectively, with a negligible contribution from the microturbulence. The C/He ratio is 0.6% but a ratio of 1% was assumed in construction of the NLTE model. Recomputation of the model for C/He=0.6% results in negligible changes to the abundances in Table 1. Abundance uncertainties are similar for the LTE analysis.

With the exception of H I, C III and the Ne I lines, the introduction of NLTE for the model atmosphere and line analysis has a minor effect on the derived abundances. The mean abundance differences in dex in the sense (LTE – NLTE) are 0.07 (C I), 0.04 (C II),  $-0.07$  (N II),  $-0.26$  (O II), and 0.81 (Ne I).

The H I lines show similar NLTE effects (LTE – NLTE) across the lines. The difference in abundance (LTE – NLTE) is about 0.33 dex. Note that, the NLTE/LTE abundance from H $\beta$  down the sequence decreases by about 0.3 dex.

The C III lines represent a fascinating issue in line formation. In the LTE analysis, the 4186.9Å 40 eV line gives an abundance that is 0.6 dex greater than that from the 4650Å triplet which provides a more plausible abundance. In NLTE, however, the abundance discrepancy is reversed: the 4186Å line gives a plausible abundance that is 0.7 dex less than that from the triplet. Nieva & Przybilla (2008) state that the sense of this reversal is expected according to their calculations for normal B stars. The magnitude of the NLTE effects and the failure of our calculations to provide consistent NLTE abundances suggests that the C III be given lower weight in the analysis.

There are small and unimportant differences between the 2006 LTE abundances and those in Table 1. Such differences arise from a combination of factors: the model atmosphere codes are different, and the derived atmospheric parameters are different. The differences in dex in the sense (TLUSTY – STERNE) are 0.12 (C I), 0.04 (C II), 0.14 (N II), 0.18 (O II) and 0.04 (Ne I).

#### 4.2. BD–9° 4395

This star’s spectrum contains absorption lines with variable profiles and variable emission lines mainly from He I, C II, and Si II transitions. These emission lines have been attributed to a shell or extended atmosphere. An extensive library of optical and ultraviolet spectra of BD–9° 4395 was discussed by Jeffery & Heber (1992) who undertook an abundance analysis using absorption lines drawn from a mean optical spectrum. Their LTE analysis led to the atmospheric parameters:  $T_{\text{eff}} = 22700 \pm 1200$  K,  $\log g = 2.55 \pm 0.10$ , and  $\xi =$

$20 \pm 5 \text{ km s}^{-1}$ . In addition to the line broadening from the high microturbulence and line profile variations, the line profiles suggested the star may be rotating at about  $40 \text{ km s}^{-1}$ .

Our high-resolution optical spectra confirm the characteristics described by Jeffery & Heber. We measure equivalent widths off our spectra. Most of the measured equivalent widths are from the 16 June 2000 spectrum. These measured equivalent widths are in fair agreement with those measured off the spectra obtained on other dates.

Our abundance analysis follows the method discussed in the previous section. Details about the majority of the lines are taken from (Pandey et al. 2006) with information on other lines of C II-III, N II-III, O II, and Ne II from the NIST database ([http://physics.nist.gov/PhysRefData/ASD/lines\\_form.html](http://physics.nist.gov/PhysRefData/ASD/lines_form.html)). The source of  $gf$ -values for Ne I lines is as given in Section 4.1.

The O II lines confirm the high microturbulence with our NLTE analyses giving  $\xi = 17.5 \pm 5 \text{ km s}^{-1}$ . This value is not sensibly different from the  $20 \text{ km s}^{-1}$  obtained by Jeffery & Heber. The microturbulence is somewhat higher than found for most other EHe stars and indicates supersonic atmospheric motions.

The He I lines are moderately sensitive to gravity. As clearly noted by Jeffery & Heber, emission affects the He I profiles to differing degrees. For example, the  $5876 \text{ \AA}$  line is in emission. Observed profiles of the  $4143 \text{ \AA}$  and  $4387 \text{ \AA}$  line are shown in Figure 6 with predicted NLTE profiles for a NLTE atmosphere of  $T_{\text{eff}} = 24300 \text{ K}$  and three different surface gravities. The predicted profiles have been convolved with a (Gaussian) profile with a FWHM of  $40 \text{ km s}^{-1}$  to represent the projected rotational velocity suggested by Jeffery & Heber. The chosen lines are those least affected by emission (Jeffery & Heber 1992). There may be indications that weak emission contaminates the red wing and, perhaps, the line core. LTE profiles shown by Jeffery & Heber predict less deep cores than the observed profiles; the NLTE profiles reproduce the line cores more closely than LTE profiles.

Ionization equilibria C II/C III, and N II/N III provide two loci in the  $(T_{\text{eff}}, \log g)$  plane (Figure 7). Inspection of this figure suggests a solution with  $T_{\text{eff}} = 24300 \pm 700 \text{ K}$  and  $\log g = 2.65 \pm 0.20 \text{ cgs}$  where we give equal weight to the C and N ionization equilibria. This effective temperature is  $1600 \text{ K}$  hotter than estimated by Jeffery & Heber. The difference is partly accounted for by the fact that the earlier (LTE) analysis included loci representing ionization equilibrium for Si II/Si IV and S II/S III and these loci of similar slope to the C and N loci fell about  $1000 \text{ K}$  to lower temperatures. Final abundances for our adopted model are given in Table 2. Mean abundances and their standard deviations are given. The rms uncertainties arising from the estimated uncertainties of the atmospheric parameters are 0.05 (C II), 0.16 (C III), 0.08 (N II), 0.20 (N III), 0.02 (O II), 0.08 (Ne I), and 0.16 (Ne II).



The LTE abundances in Table 2 were computed from a TLUSTY LTE model atmosphere with model parameters  $(T_{\text{eff}}, \log g, \xi) = (24800, 2.85, 23.0)$ . Line by line LTE abundances including the mean abundance and the line-to-line scatter are given in Table 2. These LTE abundances are quite similar to those reported by Jeffery & Heber from a different line list with different atomic data, a different model chosen from a different grid of LTE atmospheres: the differences in dex in the sense (TLUSTY – JH) are 0.22 (C II),  $-0.35$  (C III), 0.03 (N II),  $-0.01$  (N III), 0.05 (O II), 0.02 (Ne I), and  $-0.13$  (Ne II).

Corrections for NLTE effects in the sense (LTE – NLTE) are  $-0.34$  (H I), 0.11 (C II),  $-0.07$  (C III), 0.32 (N II), 0.37 (N III),  $-0.09$  (O II), 0.60 (Ne I), and  $-0.01$  (Ne II) in dex. In the case of C and Ne, the two stages of ionization treated in NLTE give consistent abundances but do not in LTE. Also, noteworthy is that the C III lines treated in NLTE give fairly consistent results but this was not the case for BD+10° 2179.

The NLTE correction (LTE – NLTE) for H I is about  $-0.34$  dex, a reversal in the NLTE correction that was provided by the analysis of BD+10° 2179. It appears that the NLTE correction (LTE – NLTE) is mainly a function of effective temperature as these stars are of similar surface gravity.

### 4.3. LSE 78, V1920 Cyg, HD 124448, and PV Tel

Neon abundances for this quartet are estimated by applying corrections to the LTE Ne abundances from Ne I lines based on the NLTE calculations computed for model atmosphere grids computed for BD+10° 2179 and BD–9° 4395. NLTE Ne abundances for LSE 78 and V1920 Cyg are estimated by interpolation in the grids of computed NLTE corrections but for HD 124448 and PV Tel an extrapolation is required. Neon LTE abundances are computed with the LTE models and the Armagh LTE code SPECTRUM (Jeffery & Heber 1992; Jeffery, Woolf & Pollacco 2001). In Tables 3, 4, 5, and 6, we give line by line LTE neon abundances including the mean abundance, and the line-to-line scatter. The estimated NLTE corrections to the LTE neon abundances of LSE 78, V1920 Cyg, HD 124448, and PV Tel are 0.73, 0.8, 0.8, and 0.88, respectively.

For LSE 78 and V1920 Cyg, the LTE Ne abundance is independent of a Ne I’s line equivalent width when the microturbulence from the 2006 paper is adopted. For HD 124448, two weak Ne I lines provide the abundance and the adopted value of the microturbulence is unimportant. In the case of PV Tel, the only Ne I lines available from our spectra are strong and the microturbulence from the 2006 paper gives a Ne abundance that is a function of a line’s equivalent width, a trend that may be removed by increasing the adopted value of

the microturbulence from the  $15\pm 4$  km s<sup>-1</sup> found in 2006 from optical N II and S II lines to 25 km s<sup>-1</sup> and then the LTE Ne abundance is  $8.53\pm 0.08$  (Table 6). An estimated NLTE correction of 0.9 dex gives the NLTE Ne abundance of 7.6.

#### 4.4. LS IV +6° 002

Abundance analysis of LS IV +6° 002 was done by Jeffery (1998) using absorption line equivalent widths drawn from the optical spectrum. This LTE analysis led to the atmospheric parameters:  $T_{\text{eff}}=31800\pm 800$  K,  $\log g=4.05\pm 0.10$ , and  $\xi = 9\pm 1$  km s<sup>-1</sup>. This is the hottest star in our sample with Ne II but not Ne I lines in its spectrum.

Here Jeffery (1998)'s equivalent width have been reanalyzed using our  $gf$ -values from (Pandey et al. 2006) and the NIST database. Two sets of model atmospheres are considered: NLTE/TLUSTY and LTE/TLUSTY. Analyses of the C III, N II, and O II lines confirm the microturbulence obtained by Jeffery with our NLTE and LTE analyses giving  $\xi$  about 9 km s<sup>-1</sup>. Ionization equilibria C II/C III, and N II/N III provide two loci in the  $(T_{\text{eff}}, \log g)$  plane (Figure 8). The He I 4471Å line that is moderately insensitive to gravity provides another locus.

Inspection of Figure 8, produced by adopting NLTE/TLUSTY models, suggests a solution with  $T_{\text{eff}}=30000\pm 800$  K and  $\log g=4.10\pm 0.15$  cgs. The He II 4686Å line suggests an effective temperature about 1000 - 2000 K hotter. Here we give more weight to the C and N ionization equilibria, and the locus provided by the He I 4471Å line. This effective temperature is 2000K cooler than estimated by Jeffery. Final abundances for our adopted model are given in Table 7. Mean abundances and their standard deviations are given. Corrections for NLTE effects in the sense (LTE – NLTE) in dex are as follows:  $-0.33$  (H I),  $0.13$  (C II),  $-0.36$  (C III),  $-0.30$  (N II),  $0.25$  (N III),  $0.14$  (O II), and  $-0.02$  (Ne II).

The LTE abundances in Table 7 were computed from a TLUSTY LTE model atmosphere. The best TLUSTY LTE model parameters are  $(T_{\text{eff}}, \log g, \xi)=(32000, 4.20, 9.0)$ . Note that, no weight is given to the C ionization equilibrium suspecting departures from LTE. Line by line LTE abundances including the mean abundance and the line-to-line scatter are given in Table 7. These LTE abundances are quite similar to those reported by Jeffery from a different line list with different atomic data, a different model chosen from a different grid of LTE atmospheres.

Our NLTE Ne abundance in Table 7 is based on Kurucz  $gf$ -values for the Ne II lines. The NLTE corrections for these Ne II lines are small being typically 0.02 dex in the sense that the NLTE abundance is higher than the LTE value. Jeffery's 1998 LTE Ne abundance

is based on  $gf$ -values that are systematically smaller than our adopted values with a mean difference of 0.7 dex. Thus our LTE Ne abundance is 0.7 dex lower than Jeffery’s value of 9.33.

## 5. Interpreting the neon and CNO abundances

### 5.1. The context

Knowledge of the chemical composition of EHe stars has become more complete in recent years. Neon adds a new constraint on proposed origins for these H-deficient stars. In order to exploit this probe fully, the Ne abundance must be considered with the reported abundances of other elements in EHe stars. A summary of He, C, N, O, Ne, and Fe abundances is given in Table 8. NLTE abundances are given for C, N, O, and Ne but not for Fe. For this review, we rely heavily on our earlier analysis (Pandey et al. 2006). Two of our seven stars were not included in the 2006 analysis and two from that analysis are not discussed here. For selected points below, we comment on abundance aspects for other EHe stars with an abundance analysis.

The following appear to be key points:

Hydrogen: Hydrogen is truly a trace element with depletion factors of  $10^3$  or greater.

Carbon/Helium ratio: The C/He ratio runs from about 0.3% to 1.0% by number for the stars in Table 8. Five cool EHe stars (Pandey et al. 2001; Pandey & Reddy 2006) and the two other EHe stars discussed by (Pandey et al. 2006) also fall within this range. Two known EHe stars fall well below the range: V652 Her with C/He=0.004% (Jeffery, Hill & Heber 1999) and HD 144941 with C/He=0.002% (Harrison & Jeffery 1997). One supposes that the scenario accounting for the stars in Table 8 and others with a similar C/He ratio will need major revision to account for V652 Her and HD 144941.

Nitrogen: The N abundance is generally equal to the sum of the initial C, N, and O abundances as inferred from an EHe’s Fe abundance and standard relations for C, N, and O dependences on initial Fe abundance for normal (i.e., H-normal) dwarfs. This is shown in Figure 9.

Oxygen: Oxygen abundances show a large spread: for example, [O/H] at [Fe/H]  $\sim 0$  runs from about +1 to  $-1$  and is, therefore, generally at odds with a simple extrapolation from the N abundances that O should be greatly depleted (Figure 10). The spread persists to lower [Fe/H] with EHe stars with [O/H]  $\simeq 0$  found at [Fe/H]  $\simeq -2$ .

Neon: Our NLTE analysis shows Ne abundances are approximately independent of a star’s Fe abundance (Figure 11). The spread in Ne abundance at a given Fe/H is about 1 dex. Qualitatively, Ne is similar to O with respect to spread and Fe-independence. Neon is not tightly correlated with the O abundance but the O-richest stars include two of the most Ne-rich and, perhaps significantly, are stars with a strong *s*-process enrichment (V1920 Cyg and LSE 78).

Mg to Ni: Abundances of these metals (relative to Fe) follow the relations determined from analyses of Galactic disk and halo stars. In particular, the so-called  $\alpha$ -elements (Mg, Si, S, Ca, and Ti) in EHe stars fall quite well on the established  $[\alpha/\text{Fe}]$  versus  $[\text{Fe}/\text{H}]$  trends.

Iron: EHe stars span the metallicity range  $[\text{Fe}/\text{H}] = -0.3$  to  $-2.0$ .

*s*-process: Several EHe stars appear enriched in *s*-process products. V1920 Cyg and LSE 78, for example, show fifty-fold overabundances of the lighter *s*-process products Y and Zr.

Other intriguing abundance anomalies are provided from analyses of RCB and HdC stars which would seem probable relatives of the EHe stars. These anomalies which are undetectable in the EHe stars because the spectroscopic signatures vanish at the higher temperatures include:

$^{18}\text{O}$ : A spectacular anomaly is the extraordinarily high  $^{18}\text{O}$  abundance seen in cool HdC and RCBs:  $^{18}\text{O}/^{16}\text{O} \simeq 0.5$  in extreme cases (Clayton et al. 2005, 2007; García-Hernández et al. 2009, 2010). Of course, the O isotopic abundance ratio requiring detection of the CO molecule is not measureable for either warm RCBs or the EHes.

Lithium: Similarly, measurement of the Li abundance demands a cool atmosphere for detection of the Li I resonance doublet at 6707 Å. Lithium is seen in one of the five HdC and in four of approximately 30 known RCBs.

Fluorine: A remarkable overabundance of F was discovered by Pandey (2006) for the cooler EHes and Pandey, Lambert & Rao (2008) for the warmer RCBs. The F I lines vanish at the higher temperatures of the hot EHes discussed here. The F abundances extend to 300 times the solar abundance and the maximum value appears to be independent of a star’s Fe abundance. There is a star-to-star spread in F abundances at a given  $[\text{Fe}/\text{H}]$ .

Minority RCBs: A few RCBs show highly anomalous  $[\text{Si}/\text{Fe}]$  and  $[\text{S}/\text{Fe}]$  ratios. Such stars were called minority RCBs by Lambert & Rao (1994) with examples including the RCB V CrA with  $[\text{Si}/\text{Fe}] \simeq [\text{S}/\text{Fe}] \simeq +2$  where  $\simeq +0.3$  is expected for normal H-rich stars of the same metallicity (Rao & Lambert 2008). None of the analyzed EHe stars has this minority characteristic but a larger sample may uncover an example. The hot RCB DY Cen, a star

known for its reluctance to decline from maximum light, is a minority star and might almost be called a EHe star.

## 5.2. The Double-degenerate scenario

### 5.2.1. A recipe

In the simplest implementation of the DD scenario, a He white dwarf (WD) merges with a C-O WD to produce a EHe star without nucleosynthesis occurring during the merger, an occurrence which we term a cold merger. Subsequent evolution of the H-deficient supergiant star is assumed not to result in further changes of surface composition. Under these assumptions, it is possible to predict the composition of the EHe star created by the merger. The merger seems certain to result in a rapidly rotating compact object. Expansion of the envelope to produce the EHe giant will through conservation of angular momentum result in a less rapidly rotating star. Here, one recalls that slowly rotating normal giants evolve from parts of the main sequence where rapidly rotating stars are common. Line profiles of the EHes indicate a high macroturbulent velocity to which the projected rotational velocity may be a significant contributor, e.g., BD-9°4395's line profiles suggest the projected rotational velocity is about  $40 \text{ km s}^{-1}$ .

In this picture, the merger involves mixing without nuclear cooking of two principal ingredients: the He WD and the former He-shell of the C-O WD.<sup>3</sup> A third potential ingredient may be provided by those layers of the C-O WD immediately below its He-shell which may be disturbed and mixed with the accreted He WD during the merger. One or both WDs before the merger may contain a thin outer layer of H-rich material but since H is very deficient in the merged star, we may neglect these H-rich layers in the following discussion of abundances of major elements resulting from a cold merger. Gravitational settling may occur in both the He and the C-O WDs ahead of the merger. Effects of settling in the He WD will be erased when the star is merged with the C-O WD. The merger event presumably stirs up the C-O WD's He shell and again the effects of gravitational settling are negated. Our recipe assumes that the He WD is thoroughly mixed with the thin He-shell of the C-O WD. Implications of mergers involving H-rich layers are explored briefly in an attempt to account for the Li-rich RCB stars. To predict the merged star's composition we need the masses and compositions of the ingredients.

---

<sup>3</sup>Here, the He WD has a He-core and is to be distinguished from a DB WD, a star with a He atmosphere but a C-O core.

### 5.2.2. *One ingredient - The He WD*

In principle, a He WD is created from low mass main sequence stars but this requires a time exceeding the age of the Galaxy. Thus, the He WD in a DD scenario must be a product of a binary system experiencing mass loss and probably mass transfer. Iben, Tutukov & Yungelson (1997) predict the mass distribution of He and C-O WDs expected to result from evolution of close binaries:  $M(\text{He}) \simeq 0.3 \pm 0.1M_{\odot}$  and  $M(\text{C-O}) \simeq 0.6 \pm 0.1M_{\odot}$ . Such a He WD’s composition is dominated by He and N: the mass fraction  $\mu(\text{He})$  of He is essentially unity and, thanks to H-burning by the CNO-cycles, the N abundance is the sum of the initial C, N, and O abundances, say,  $\mu(\text{CNO})_0$  where 0 denotes that the initial C, N, and O abundances will be dependent on the initial metallicity (here inferred from the Fe abundance). Mass fractions of C and O in the He white dwarf may be taken to be zero. Heavier elements will have their initial mass fractions. Thus, the mass of helium and nitrogen contributed to the merged star assuming a conservative cold merger are essentially  $M(\text{He})$  and  $\mu(\text{CNO})_0M(\text{He})$ , respectively.

### 5.2.3. *Another ingredient - The He shell of the C-O WD*

For the He shell of the C-O WD, estimates of the mass and composition of the He shell should be obtained from calculations of binary star evolution that result in appropriate He and C-O WD pairs, but understandably such calculations appear not to have been reported. Therefore, we take estimates from calculations for the inner regions of single stars in their AGB phase prior to loss of their H-rich envelopes. In such cases, the mass of the He shell is approximately  $0.02M_{\odot}$  for 1-3  $M_{\odot}$  stars but decreases to  $0.002M_{\odot}$  for the more massive stars. We denote this mass by  $M(\text{C-O:He})$ .

Early calculations showed that the He shell was primarily comprised of  $^4\text{He}$  and  $^{12}\text{C}$  with mass fractions of about 0.75 and 0.20, respectively, with  $^{16}\text{O}$  having a mass fraction of only about 0.01 (Schönberner 1979). We make use of calculations by Karakas (2010) (and private communication) for stars with masses of 1 to 6  $M_{\odot}$  and with initial compositions  $Z=0.0001$  to 0.02. Adopted compositions are the average of the He-shell’s composition just prior to third dredge-up and at the point at which the star leaves the AGB. Mass fractions of  $^4\text{He}$ ,  $^{12}\text{C}$  and  $^{16}\text{O}$  are consistent with Schönberner’s estimates. In Karakas et al.’s calculations, the He mass fraction  $\mu(\text{He})_{\text{C-O:He}}$  is about 0.75, almost independent of mass and composition. The  $^{12}\text{C}$  mass fraction  $\mu(\text{C})_{\text{C-O:He}} \simeq 0.20$ , again with little dependence on mass and composition.  $^{14}\text{N}$  is effectively cleansed from the region and we take its mass fraction to be zero. The  $^{16}\text{O}$  mass fraction is  $\mu(\text{O})_{\text{C-O:He}} \simeq 0.005$ .

Of particular interest to attempts to match the EHe compositions is that the He shell has enhanced  $^{22}\text{Ne}$  and  $^{19}\text{F}$  abundances. Mass fractions of these two nuclides are dependent on the mass of the initial star but are not particularly sensitive to the initial metal mass fraction  $Z$ . The  $^{22}\text{Ne}$  is synthesised from  $^{14}\text{N}$  by  $\alpha$ -capture, first to  $^{18}\text{O}$  and then to  $^{22}\text{Ne}$ . Its abundance peaks in stars of about  $3M_{\odot}$  reaching a mass fraction of about 0.05, a value not greatly dependent on the initial metallicity of the star. The  $^{22}\text{Ne}$  mass fraction decreases to lower initial stellar masses by a factor that is metallicity dependent: at  $Z = 0.008$ , the mass fraction for a  $1M_{\odot}$  star is a factor of six below that for a  $3M_{\odot}$  star. At higher masses than  $3M_{\odot}$ ,  $^{22}\text{Ne}$  is destroyed by  $\alpha$ -particles and converted to  $^{25}\text{Mg}$  and  $^{26}\text{Mg}$ .

Synthesis of  $^{19}\text{F}$  occurs from  $^{15}\text{N}$  by  $^{15}\text{N}(\alpha, \gamma)^{19}\text{F}$  in competition with  $^{19}\text{F}(\alpha, \text{p})^{22}\text{Ne}$  with  $^{15}\text{N}$  produced by either  $^{14}\text{N}(\text{n}, \text{p})^{14}\text{C}(\alpha, \gamma)^{18}\text{O}(\text{p}, \alpha)^{15}\text{N}$  or  $^{14}\text{N}(\alpha, \gamma)^{18}\text{F}(\beta^+)^{18}\text{O}(\text{p}, \alpha)^{15}\text{N}$  with neutrons from  $^{13}\text{C}(\alpha, \text{n})^{16}\text{O}$  and protons from  $^{14}\text{N}(\text{n}, \text{p})^{14}\text{C}$ . The  $^{19}\text{F}$  mass fraction is a maximum for  $M \simeq 3M_{\odot}$  decreasing by about factors of 20-30 for  $1M_{\odot}$  and 10 for  $6M_{\odot}$ . At maximum, the mass fraction  $\mu(\text{F})_{\text{C-O:He}} \simeq 1 \times 10^{-4}$ .

Other series of calculations for AGB stars introduce convective overshoot at the base of the He-burning thermal pulse in the He shell.<sup>4</sup> Overshoot necessarily brings more  $^{16}\text{O}$  (and  $^{12}\text{C}$ ) into the shell from the top of the C-O core. Various implementations of convective overshoot have been reported in the literature: for example, Herwig (2000) (see also Herwig (2006)) reports for a star of initial mass  $3M_{\odot}$  that the He shell at the last thermal pulse has mass fractions of 0.41 and 0.18 for  $^{12}\text{C}$  and  $^{16}\text{O}$ , respectively, showing an order of magnitude increase in the  $^{16}\text{O}$  mass fraction from the calculation without this convective overshoot. One may anticipate the possibility that O abundances in EHe stars may offer an indirect test of calculations with and without convective overshoot extending into the C-O core.

#### 5.2.4. *Mixing the ingredients*

With estimates of the compositions of the two principal ingredients, we may predict the outcomes of a cold merger. As noted above, we may set H aside because its abundance in the EHe star can be readily accounted for by adding a small H-rich skin to the He WD and/or the C-O WD. Estimates for other elements are as follows:

The C/He ratio: Helium is provided overwhelmingly by the He WD and C exclusively

---

<sup>4</sup>This episode of convective overshoot is to be distinguished from convective overshoot at the base of the H-rich convective envelope into the top of the He shell of an AGB star. This affects operation of the *s*-process in the He shell between thermal pulses and also the composition of the surface layers - see Karakas, Campbell & Stancliffe (2010) for a discussion.

by the C-O WD’s He shell. The predicted C/He ratio by number is

$$\frac{\text{C}}{\text{He}} \simeq \frac{A(\text{He})}{A(\text{C})} \frac{\mu(\text{C})_{\text{C-O:He}} M(\text{C-O:He})}{M(\text{He})} \quad (1)$$

where  $A(X)$  denotes the atomic weight of  $X$ .

With  $\mu(\text{C})_{\text{C-O:He}} \simeq 0.2$ ,  $M(\text{C-O:He}) \simeq 0.02M_{\odot}$ , and  $M(\text{He}) \simeq 0.3M_{\odot}$ ,  $\text{C/He} \simeq 0.4\%$ . Since the observed range of the C/He ratio is from 0.3% to 1.0%, our prediction accounts well for the lower end of the observed range. It is possible to account for the upper end with not implausibly different choices for the three variables. If additional  $^{12}\text{C}$  is needed, it may be provided by the third ingredient, the ‘surface’ layers of the C-O white dwarf where the  $^{12}\text{C}$  mass fraction may approach 0.5 to 0.8: For example, an additional contribution of  $0.01M_{\odot}$  with a  $^{12}\text{C}$  mass fraction of 0.5 raises the C/He to 1% after the merger.

Although not present in our sample of EHes for which we have derived the Ne abundance, two EHes – V652 Her and HD 144941 - as noted above have lower C/He ratios by two orders of magnitude:  $\text{C/He} \simeq 0.003\%$ . An interpretation is that these stars result from a DD scenario involving a pair of He white dwarfs. An alternative possibility based on the above equation is that the C-O white dwarf in the merger had an unusually small He shell around the C-O white dwarf, as might be anticipated for a star of intermediate mass.

The N abundance: Nitrogen, a product of CNO-cycling, is contributed by the He WD which also is the dominant contributor of mass to the merger and, hence, the leading supplier of a reference element such as Fe. These circumstances explain quite naturally why the observed N abundance in stars of different Fe abundance is equal to the sum of the initial C, N, and O abundances.

The oxygen abundance: The O abundance is given by

$$\frac{\text{O}}{\text{He}} \simeq \frac{A(\text{He})}{A(\text{O})} \frac{\mu(\text{O})_{\text{C-O:He}} M(\text{C-O:He})}{M(\text{He})} \quad (2)$$

With  $\mu(\text{O})_{\text{C-O:He}} \simeq 0.005$ ,  $M(\text{C-O:He}) \simeq 0.02M_{\odot}$ , and  $M(\text{He}) \simeq 0.3M_{\odot}$ ,  $\text{O/He} \simeq 0.008\%$  corresponding to an abundance  $\log \epsilon(\text{O}) \simeq 7.5$ , a value at the lower bound of the observed abundances.

There appear to be two possibilities by which to increase the predicted O abundances: (i) add the third ingredient, i.e., surface layers from the C-O WD, when, for example, a mass of  $0.01M_{\odot}$  and an  $^{16}\text{O}$  mass fraction of 0.5 raises the O abundance to 9.2, the maximum observed value; (ii) increase the O mass fraction in the He shell to 0.2, a value expected



if convective overshoot during the AGB phase extends into the C-O core, and then the predicted O abundance is 8.1. Both of these possibilities may depend on individual properties of the stars involved in the merger and, thus, might account for the observed spread in O abundances among EHe (and RCB) stars. As long as the responsible agent is not metallicity dependent, the lack of a trend of O abundance with metallicity is accounted for.

The Neon abundance: The Ne abundance is

$$\frac{\text{Ne}}{\text{He}} \simeq \frac{A(\text{He})}{A(^{22}\text{Ne})} \frac{\mu(\text{Ne})_{\text{C-O:He}} M(\text{C-O:He}) + \mu(\text{Ne})_0 M(\text{He})}{M(\text{He})} \quad (3)$$

where contributions from the He-shell of the C-O white dwarf and the original Ne content of the He white dwarf are included.

With  $\mu(\text{Ne})_{(\text{C-O:He})} \simeq 0.05$ ,  $M(\text{C-O:He}) \simeq 0.02M_{\odot}$  and  $M(\text{He}) \simeq 0.3M_{\odot}$ ,  $\text{Ne/He} \simeq 0.06\%$  corresponding to an abundance  $\log \epsilon(\text{Ne}) \simeq 8.4$ , a value equal to the upper bound of the observed abundances (Table 8, and Figure 11). Lower Ne abundances are readily achieved because the Ne mass fraction is lower in all but  $3M_{\odot}$  stars. Karakas’s predictions encompass an order of magnitude range in Ne mass fractions and the observed Ne abundances from our (small) sample of EHe stars show a factor of five spread. In all cases but two (HD 124448 and PV Tel), the Ne abundance is appreciably greater than the presumed initial abundance based on the Fe abundance and likely relation between initial Ne and Fe abundances.

The Fluorine abundance: Fluorine is not detectable in these hot EHes but its abundance is known for cooler EHes and the warmer RCBs, as noted above. The maximum mass fraction for F in the He shell gives an abundance  $\log \epsilon(\text{F}) \simeq 5.7$  but observed abundances are about 1 dex higher. This may suggest that the nucleosynthesis of F has been underestimated in the He shell, or the derived F abundance for cooler EHes has been overestimated. This gap might also be bridged by NLTE calculations of F I line formation; such calculations for Ne I, an atom with a not dissimilar atomic structure, show an almost one dex reduction of the observed LTE abundances.

The  $^{18}\text{O}$  abundance: Extraordinary amounts of  $^{18}\text{O}$  are present with the  $^{18}\text{O}$  abundance exceeding that of  $^{16}\text{O}$  in several stars. The  $^{18}\text{O}/^{16}\text{O}$  ratio is higher and the  $^{18}\text{O}$  abundance lower in most of the RCBs where CO lines are detectable; García-Hernández et al. (2010) speculate that a late dredge-up in a HdC star is responsible for these differences between HdC and RCB stars. These high  $^{18}\text{O}$  abundances cannot be explained by the two or even the three ingredient recipe describing the DD scenario as a cold merger. One may wonder if the C-O WD’s He shell has a composition that is not a complete replica of a He shell of a single star, the model we have adopted for these calculations. Perhaps, the synthesis of

$^{22}\text{Ne}$  from  $^{14}\text{N}$  is incomplete and some  $^{18}\text{O}$  remains. But one wonders if this suspicion may be reconciled with the fact that the maximum  $^{18}\text{O}$  abundances for the HdC stars ( $\log \epsilon(^{18}\text{O}) \simeq 8.6$ ) are greater than the Ne abundances ( $\log \epsilon(\text{Ne}) \simeq 8.5$ ) in the EHe stars. Is such fine tuning possible?

Clayton et al. (2005) considered  $^{18}\text{O}$  synthesis to occur by nuclear processing during accretion of He WD material by the C-O WD. In the processing,  $^{14}\text{N}$  is converted to  $^{18}\text{O}$  by  $\alpha$ -capture. The observed  $^{18}\text{O}$  abundances are not sufficiently great to have sensibly reduced the  $^{14}\text{N}$  abundances: the  $^{18}\text{O}$  abundances are factors of 4 to 20 less than the  $^{14}\text{N}$  abundances. However, fine-tuning is required in order not to deplete entirely the  $^{14}\text{N}$  supply and also to prevent conversion of significant amounts of  $^{18}\text{O}$  by  $\alpha$ -capture to  $^{22}\text{Ne}$ .

The  $s$ -process: Enrichment of  $s$ -process nuclides likely in the C-O WD's He shell will be diluted by the absence of enrichment in the He WD. Thus, the enrichment will be diluted by about an order or magnitude if  $M(\text{He}) \simeq 0.3M_{\odot}$  and  $M(\text{He})_{\text{C-O}} \simeq 0.02M_{\odot}$ . Two of the EHes are observed enriched in Y and Zr 50-fold and another 10-fold. Other stars have lower enrichment levels. Although a 100- to 500-fold enrichment is within expected levels for isolated AGB stars, the general lack of a large  $s$ -process enrichment of these EHes, as well as the cool EHes (Pandey et al. 2001) and the warmer RCBs (Asplund et al. 2000) implies that the He shell of the C-O WD was not itself greatly  $s$ -process enriched. This would seem to confirm suspicions that the He shells participating in the DD scenario may not be near-copies of He shells of isolated AGB stars.

Lithium: Lithium is, of course, not observable in EHe stars but its presence in several RCBs and in one of five known HdCs suggests that it is probably present in at least some EHe stars. Therefore, the challenge exists to account for the Li abundance in the DD scenario.

An initial supposition is that the Li was present in the H-rich skin around the white dwarfs. Then, the observed Li/H ratio for the RCB star is the mass-weighted mean of the Li/H ratio in the two H-rich skins. For the four RCBs with Li,  $\log \text{Li}/\text{H}$  ranges from  $-1.7$  for RZ Nor to  $-4.8$  for SU Tau (Asplund et al. 2000) or Li abundances of 10.3 to 7.2 on the usual logarithmic scale where the H abundance is 12.0. Such extraordinarily high Li abundances are observed nowhere else: for example, the Li-rich carbon stars have Li abundances *only* (!) in the range 3 to 5 (Abia et al. 1999).

In the usual scheme of Li synthesis known as the Cameron-Fowler mechanism (Cameron & Fowler 1971), Li as  $^7\text{Li}$  is synthesised from  $^3\text{He}$  by the chain  $^3\text{He}(^4\text{He}, \gamma)^7\text{Be}(e^-, \nu)^7\text{Li}$ . The potential reservoir of  $^3\text{He}$  is the star's original supply of  $^3\text{He}$  and  $^2\text{H}$  (which is burnt to  $^3\text{He}$  in pre-main sequence phase) and additional  $^3\text{He}$  provided by operation of the  $pp$ -chains in low mass main sequence stars. The original  $^3\text{He}/\text{H}$  after  $^2\text{H}$  burning will have been about  $2 \times 10^{-5}$ . In low

mass stars, a layer of enriched  $^3\text{He}$  exists outside the H-burning core. The abundance can reach  $10^{-3}$  of that of H over a shell about  $0.2M_{\odot}$  in thickness (Iben 1967). Protons are not directly involved in the Cameron-Fowler mechanism but the temperature of the synthesis site may be influenced by the mass exterior to the site.

In the case of the Li-rich normal carbon stars, the site is the high temperature base of the H-rich convective envelope in an intermediate-mass AGB star. In this environment, the observed range of Li abundances can be achieved. To achieve a higher abundance (i.e., a higher Li/H ratio), it seems necessary to reduce the mass of the H into which products ( $^7\text{Be}$  and then  $^7\text{Li}$ ) of  $^3\text{He}$  consumption are mixed. Efficiency of  $^7\text{Li}$  production might be maximised were the  $^3\text{He}$  consumed in a layer completely devoid of H; this would remove the loss of  $^7\text{Be}$  and  $^7\text{Li}$  by proton capture but these nuclides would still be prone to destruction by  $\alpha$ -capture. Further exploration of  $^7\text{Li}$  synthesis will require very detailed calculations of nucleosynthesis in close binary systems.

### 5.3. The Final-flash scenario

Several classes of H-deficient hot luminous post-AGB stars are believed to have resulted from a final-flash scenario. Compositions of these stars offer a direct point of comparison for the EHe (also RCB and HdC) stars and, therefore, a test of the final-flash scenario as an origin for some EHe stars.

A valuable review of the observed compositions and theoretical origins of hot H-deficient post-AGB stars was provided by Werner & Herwig (2006). Their Table 1 clearly shows that the several families ([WCL], [WCE], [WC]-PG1159, and PG1159) of such post-AGB stars have compositions differing in several distinctive ways from the compositions of EHe and RCB stars. In particular, the relative C/He ratio is quite different. The (He,C) mass fractions are roughly in the range (0.30,0.60) to (0.85,0.15) whereas the EHe stars are close to (0.98,0.02) (Werner et al. 2008). This contrast is, of course, very largely attributable to the He contribution by the He white dwarf to the DD scenario. Several of the post-AGB stars show a residue of their original H with a mass fraction of as much as 0.35, but a lower value is more common. (These are hot stars and, therefore, detection of H lines is difficult.) In other respects, the compositions of the post-AGB and EHe stars are more similar: the O mass fractions show a star-to-star spread but the highest value for a post-AGB star (0.20, Werner et al. (2008)) is several times higher than the maximum value for a EHe. The F and Ne abundances are similar for the two groups of stars.

Theoretical final flash models are discussed by Werner & Herwig (2006). These models

differ as to when the He-shell flash (thermal pulse) occurs that restores the star to the post-AGB track as a EHe-like star. If the thermal pulse occurs when the star is on the AGB, it is termed a AFTP and may account for the relatively H-rich stars known as hybrid-PG1159 stars. If the thermal pulse occurs in the post-AGB period of approximately constant luminosity, it is a LTP (L=Late) and is predicted to create a H-deficient star with some H, say a mass fraction of about 0.02. FG Sge may have experienced a LTP - recently! Finally, if the thermal pulse is delayed until the star is on the WD cooling track, it is a VLTP (V=very). Sakurai’s object is considered to have undergone a VLTP - very recently! Although these post-AGB final flash scenarios fail to account for the EHe’s, one may note some similarities with the ideas behind the DD scenario. In particular, convective extramixing into the ‘surface’ layers of the C-O core is invoked in both cases to account for the spread in the O abundances, and high F and Ne abundances in the He shell around the C-O core of the AGB star **to** explain the F and Ne overabundances in both kinds of H-deficient stars.

## 6. Concluding remarks

Understanding the origins of peculiar stars often awaits recognition of predecessors and descendants along the evolutionary sequence. The sequence may provide clues not always provided by even detailed observational studies of a single class of peculiar star in the sequence. Even more important than expanded observational studies is the development of theoretical understanding of relevant stellar models and associated nucleosynthesis. The EHe stars illustrate well these remarks.

The first EHe HD 124448 was discovered by Popper (1942) at the McDonald Observatory and this was followed ten years later by discovery of PV Tel, alias HD 168476, by Thackeray & Wesselink (1952) at the Radcliffe Observatory. Today, the register of EHe’s totals about 30 (Jeffery 1996).<sup>5</sup> Today, the chemical compositions of EHe stars are quite well determined with our estimates of Ne abundances adding one more data point. Similarities in composition argue for an evolutionary link between EHe and RCB stars and less convincingly between these stars and the HdC stars of which only five are known and their spectra blessed with a rich array of molecular lines render accurate abundance analysis difficult. Theoretical ideas have centered on two possibilities: the DD- and the FF-scenarios.

While the FF scenario may account for H-deficient stars like FG Sge and Sakurai’s object (as noted above), the argument eliminating it as the origin of EHe stars is a fusion of two principal points. First, the compositions of H-deficient central stars of planetary nebulae

---

<sup>5</sup>H-deficient binaries such as KS Per and  $\nu$  Sgr are an unrelated and even rarer type of star.

differ in critical aspects from those of EHe stars. As noted in Section 5.3, the He and C mass fractions of the central stars differ greatly from these quantities as found for EHe (and RCB) stars. Second, the observed compositions of the central stars are reasonably well accounted for by models of final He-shell flashes in post-AGB stars. Thus, a safe conclusion would appear to be: the FF scenario cannot account for the EHe stars.

Identification of the EHe (and RCB) stars with the DD scenario depends on the correspondence between the measured chemical compositions and semi-quantitative theoretical estimates resulting from the merger of a He WD with a C-O WD. Predictions for a cold merger seem especially sensitive to the adopted composition of the He-shell around the C-O WD before the merger and the extent to which mixing during the merger may incorporate material from the surface layers of the C-O WD. An additional uncertainty concerns the extent of nucleosynthesis occurring during the merger; the proposal that the  $^{18}\text{O}$  seen in cool HdC and RCB stars is synthesised from  $^{14}\text{N}$  during the merger was noted (Clayton et al. 2007).

Although work remains for quantitative spectroscopists to do, we close with the thought that the larger challenges remain in the area of theoretical modelling of single stars in order to refine prediction for the several forms of the FF scenario and of double stars that through common envelope stages and mass loss provide the necessary stage for the DD scenario of a close binary of a He and a C-O WD that merge with possibly a concluding episode of nucleosynthesis to provide a EHe, RCB, or a HdC.

We thank the referee for a constructive report. We are indebted to Amanda Karakas for providing details of her calculations of AGB stars. We thank Katia Cunha for providing her Ne I line list for HD 35299. GP thanks Baba Verghese for the help provided in installing the TLUSTY/SYNSPEC codes. GP is thankful to Carlos Allende Prieto for his useful suggestions in making the TLUSTY models. We thank Ivan Hubeny for testing the convergence of one of our NLTE TLUSTY model, and for all the discussions with him. GP is also thankful to Simon Jeffery for making available Armagh LTE and other related codes. Travel support for GP to visit UT Austin and McDonald Observatory where a part of this work was carried out was provided by the Isabel McCutcheon Harte Centennial Chair. DLL thanks the Robert A. Welch Foundation for support through grant F-634.

## REFERENCES

- Abia, C., Pavlenko, Y., & de Laverny, P. 1999, *A&A*, 351, 273
- Asplund, M., Gustafsson, B., Lambert, D. L., & Rao, N. K. 2000, *A&A*, 353, 287
- Auer, L. H., & Mihalas, D. 1973, *ApJ*, 184, 151
- Blöcker, T. 2001, *Ap&SS*, 275, 1
- Clayton, G. C., Herwig, F., Geballe, T. R., Asplund, M., Tenenbaum, E. D., Engelbracht, C. W., & Gordon, K. D. 2005, *ApJ*, 623, L141
- Clayton, G. C., Geballe, T. R., Herwig, F., Fryer, C., & Asplund, M. 2007 *ApJ*, 662, 1220
- Cunha, K., Hubeny, I., & Lanz, T. 2006, *ApJ*, 647, L143
- Drilling, J. S., Jeffery C. S., & Heber, U. 1998, *A&A*, 329, 1019
- Cameron, A.G.W., & Fowler, W.A. 1971, *ApJ*, 164, 111
- García-Hernández, D. A., Hinkle, K. H., Lambert, D. L., & Eriksson, K. 2009, *ApJ*, 696, 1733
- García-Hernández, D. A., Lambert, D. L., Rao, N. K., Hinkle, K. H., & Eriksson, K. 2010, *ApJ*, 714, 144
- Harrison, P.M., & Jeffery, C.S. 1997, *A&A*, 323, 177
- Herwig, F. 2000, *A&A*, 360, 952
- Herwig, F. 2001, *Ap&SS*, 275, 15
- Herwig, F. 2006, *Proceedings of the International Symposium on Nuclear Astrophysics - Nuclei in the Cosmos - IX. 25-30 June 2006, CERN*, 206
- Hubeny, I. 1988, *Comput. Phys. Commun.*, 52, 103
- Hubeny, I., Hummer, D. G., & Lanz, T. 1994, *A&A*, 282, 151
- Hubeny, I., & Lanz, T. 1995, *ApJ*, 439, 875
- Hubeny, I., Lanz, T., & Jeffery, C. S. 1994, *SYNSPEC: a User's Guide*, in *Newsl. on Analysis of Astronomical Spectra 20* (St. Andrews Univ.)
- Iben, I., Jr. 1967, *ApJ*, 147, 624

- Iben, I., Jr., Kaler, J. B., Truran, J. W., & Renzini, A. 1983, *ApJ*, 264, 605
- Iben, I., Jr., & Tutukov, A. V. 1984, *ApJS*, 54, 335
- Iben, I., Jr., Tutukov, A. V., & Yungelson, L. R. 1996, *ApJ*, 456, 750
- Iben, I. Jr., Tutukov, A. V., & Yungelson, L. R. 1997, *ApJ*, 475, 291
- Jeffery C. S. 1996, *ASP Conf. Ser.* 96, 152
- Jeffery, C. S. 1998, *MNRAS*, 294, 391
- Jeffery, C. S., & Heber, U. 1992, *A&A*, 260, 133
- Jeffery, C. S., & Heber, U. 1993, *A&A*, 270, 167
- Jeffery, C. S., & Harrison, P. M. 1997, *A&A*, 323, 393
- Jeffery, C. S., Hamill, P. J., Harrison, P. M., & Jeffers, S. V. 1998, *A&A*, 340, 476
- Jeffery, C. S., Hill, P. W., & Heber, U. 1999, *A&A*, 346, 491
- Jeffery, C. S., Woolf, V. M., & Pollacco, D. L. 2001, *A&A*, 376, 497
- Jeffery C. S. 2008, *ASP Conf. Ser.* 391, 53
- Karakas, A. I. 2010, *MNRAS*, 403, 1413
- Karakas, A. I., Campbell, S. W., Stancliffe, R. J. 2010, *ApJ*, 713, 374
- Lambert, D. L., & Rao, N. K. 1994, *JApA*, 14, 47
- Lanz, T., & Hubeny, I. 2003, *ApJS*, 146, 417
- Lanz, T., & Hubeny, I. 2007, *ApJS*, 169, 83
- McCarthy, J. K., Sandiford, B. A., Boyd, D., & Booth, J. 1993, *PASP*, 310, 881
- Morel, T., & Butler, K. 2008, *A&A*, 487, 307
- Nieva, M. F., & Przybilla, N. 2008, *A&A*, 481, 199
- Pandey, G., Rao, N. K., Lambert, D. L., Jeffery, C. S., & Asplund, M. 2001, *MNRAS*, 324, 937
- Pandey, G., Lambert, D. L., Jeffery, C. S., & Rao, N. K. 2006, *ApJ*, 638, 454

- Pandey, G., & Reddy, B. E. 2006, MNRAS, 369, 1677
- Pandey, G. 2006, ApJ, 648, L143
- Pandey, G., Lambert, D. L., & Rao, N. K. 2008, ApJ, 674, 1068
- Popper, D. M. 1942, PASP, 54, 160
- Rao, N. K., & Lambert, D. L. 1996, ASP Conf. Ser. 96, 43
- Rao, N. K., Sriram, S., Gabriel, F., Prasad, B. R., Samson, J. P. A., Jayakumar, K., Srinivasan, R., Mahesh, P. K., & Giridhar, S. 2004, Asian Journal of Physics, 13, 267
- Rao, N. K., Sriram, S., Jayakumar, K., & Gabriel, F. 2005, JAA, 26, 331
- Rao, N. K., & Lambert, D. L. 2008, MNRAS, 384, 477
- Ryde, N., & Lambert, D. L., 2004, A&A, 415, 559
- Saio, H., & Jeffery, C. S. 2002, MNRAS, 333, 121
- Schönberner, D. 1979, A&A, 79, 108
- Seaton, M. J. 1998, J. Phys. B: At. Mol. Opt. Phys, 31, 5315.
- Thackeray, A. D., & Wesselink, A. J. 1952, The Observatory, 72, 248
- Tull, R. G., MacQueen P. J., Sneden, C., & Lambert, D. L. 1995, PASP, 107, 251
- Webbink, R. F. 1984, ApJ, 277, 355
- Werner, K., & Herwig, F. 2006, PASP, 118, 183
- Werner, K., Rauch, T., Reiff, E., & Kruk, J. W. 2008, ASP Conf. Ser. 391, 109
- Wiese, W. L., Smith, M. W., & Glennon, B. M. 1966, NSRDS–NBS 4



Table 1. Photospheric line by line NLTE and LTE abundances, and the line’s measured equivalent width ( $W_\lambda$ ) in mÅ for BD+10°2179

Line	$\chi$		$W_\lambda$ (mÅ)	$\log \epsilon(X)$	
	(eV)	$\log gf$		NLTE <sup>a</sup>	LTE <sup>b</sup>
H I $\lambda$ 3970.072	10.199	−0.993	90	8.26	8.60
H I $\lambda$ 4101.734	10.199	−0.753	146	8.28	8.60
H I $\lambda$ 4340.462	10.199	−0.447	242	8.32	8.64
H I $\lambda$ 4861.323	10.199	−0.020	430	8.54	8.88
Mean...	...	...	...	8.35±0.13	8.68±0.13
C I $\lambda$ 4932.049	7.685	−1.658	13	9.33	9.41
C I $\lambda$ 5052.167	7.685	−1.303	28	9.37	9.42
Mean...	...	...	...	9.35±0.03	9.42±0.01
C II $\lambda$ 3918.980	16.333	−0.533	286	9.08	9.30
C II $\lambda$ 3920.690	16.334	−0.232	328	9.01	9.28
C II $\lambda$ 4017.272	22.899	−1.031	43	9.40	9.40
C II $\lambda$ 4021.166	22.899	−1.333	27	9.40	9.40
C II $\lambda$ 4306.330	21.150	−1.684	46	9.25	9.32
C II $\lambda$ 4307.581	20.150	−1.383	77	9.33	9.42
C II $\lambda$ 4313.100	23.120	−0.373	83	9.40	9.38
C II $\lambda$ 4317.260	23.120	−0.005	113	9.35	9.36
C II $\lambda$ 4318.600	23.120	−0.407	80	9.40	9.38
C II $\lambda$ 4321.650	23.120	−0.901	45	9.43	9.41
C II $\lambda$ 4323.100	23.120	−1.105	45	9.64	9.62
C II $\lambda$ 4637.630	21.150	−1.229	75	9.21	9.27
C II $\lambda$ 4867.066	19.495	−1.781	35	9.27	9.10
C II $\lambda$ 5032.128	20.922	−0.143	174	9.40	9.45
C II $\lambda$ 5035.943	20.920	−0.399	113	9.09	9.14
C II $\lambda$ 5125.208	20.150	−1.597	51	9.36	9.40
C II $\lambda$ 5126.963	20.150	−1.899	32	9.36	9.40
C II $\lambda$ 5137.257	20.701	−0.911	91	9.32	9.36
C II $\lambda$ 5139.174	20.704	−0.707	118	9.38	9.43
C II $\lambda$ 5143.495	20.704	−0.212	166	9.31	9.38
C II $\lambda$ 5145.165	20.710	+0.189	207	9.34	9.31
C II $\lambda$ 5151.085	20.710	−0.179	169	9.37	9.37
Mean...	...	...	...	9.32±0.14	9.36±0.11
C III $\lambda$ 4186.900	40.010	+0.918	19	9.29	9.99
C III $\lambda$ 4647.420	29.535	+0.070	51	10.01?	9.39
C III $\lambda$ 4650.250	29.535	−0.151	42	10.05?	9.40
C III $\lambda$ 4651.470	29.535	−0.629	27	10.15?	9.43
Mean...	...	...	...	9.29±0.00	9.41±0.02
N II $\lambda$ 3842.180	21.150	−0.692	30	8.21	8.13
N II $\lambda$ 3955.851	18.466	−0.813	68	8.14	8.15
N II $\lambda$ 3994.996	18.498	+0.208	139	7.87	7.95
N II $\lambda$ 4179.670	23.250	−0.204	23	8.29	8.12
N II $\lambda$ 4227.740	21.600	−0.061	42	8.07	7.95
N II $\lambda$ 4447.030	20.411	+0.228	75	7.94	7.87
N II $\lambda$ 4507.560	20.666	−0.817	25	8.24	8.12
N II $\lambda$ 4601.480	18.468	−0.428	79	8.00	8.00

Table 1—Continued

Line	$\chi$		$W_\lambda$ (mÅ)	$\log \epsilon(X)$	
	(eV)	$\log gf$		NLTE <sup>a</sup>	LTE <sup>b</sup>
N II $\lambda$ 4607.160	18.464	−0.507	73	8.01	8.01
N II $\lambda$ 4613.870	18.468	−0.665	61	8.02	8.00
N II $\lambda$ 4643.090	18.484	−0.359	88	8.05	8.06
N II $\lambda$ 4654.531	18.497	−1.404	20	8.04	7.99
N II $\lambda$ 4667.208	18.497	−1.533	20	8.17	8.12
N II $\lambda$ 4674.908	18.497	−1.463	19	8.07	8.02
N II $\lambda$ 4779.720	20.650	−0.587	34	8.27	8.14
N II $\lambda$ 4781.190	20.650	−1.308	9	8.22	8.10
N II $\lambda$ 4788.130	20.650	−0.363	35	8.07	7.94
N II $\lambda$ 4810.310	20.660	−1.084	17	8.35	8.21
N II $\lambda$ 4895.117	17.877	−1.338	18	7.76	7.72
N II $\lambda$ 5002.700	18.480	−1.022	42	8.16	8.09
N II $\lambda$ 5007.328	20.940	+0.171	52	7.98	7.84
N II $\lambda$ 5010.620	18.470	−0.607	71	8.12	8.08
N II $\lambda$ 5025.659	20.666	−0.547	28	8.17	8.03
N II $\lambda$ 5045.090	18.460	−0.407	87	8.10	8.07
Mean...	...	...	...	8.10±0.14	8.03±0.11
O II $\lambda$ 4072.157	25.643	+0.552	26	7.92	7.60
O II $\lambda$ 4185.449	28.351	+0.604	11	8.14	7.69
O II $\lambda$ 4189.789	28.354	+0.717	20	8.47	7.99
O II $\lambda$ 4336.860	22.973	−0.763	11	7.93	7.69
O II $\lambda$ 4345.567	22.979	−0.346	18	7.81	7.59
O II $\lambda$ 4349.426	22.993	+0.060	32	7.79	7.61
O II $\lambda$ 4366.888	22.993	−0.348	15	7.71	7.49
O II $\lambda$ 4414.901	23.435	+0.172	33	7.88	7.66
O II $\lambda$ 4416.973	23.413	−0.077	26	7.97	7.72
O II $\lambda$ 4641.817	22.973	+0.055	32	7.87	7.69
O II $\lambda$ 4649.143	22.993	+0.308	41	7.79	7.65
Mean...	...	...	...	7.93±0.21	7.67±0.12
Ne I $\lambda$ 5852.488	16.850	−0.490	61	7.78	8.54
Ne I $\lambda$ 6074.338	16.670	−0.500	66	7.87	8.56
Ne I $\lambda$ 6143.063	16.620	−0.100	115	7.84	8.64
Ne I $\lambda$ 6163.594	16.710	−0.620	65	7.99	8.69
Ne I $\lambda$ 6266.495	16.710	−0.370	97	7.98	8.77
Ne I $\lambda$ 6334.428	16.620	−0.320	90	7.91	8.63
Ne I $\lambda$ 6382.992	16.670	−0.240	103	7.89	8.70
Ne I $\lambda$ 6402.246	16.620	+0.330	163	7.68	8.73
Ne I $\lambda$ 6506.528	16.670	−0.030	121	7.81	8.68
Ne I $\lambda$ 7032.413	16.620	−0.260	116	7.95	8.86
Mean...	...	...	...	7.87±0.10	8.68±0.10

<sup>a</sup>( $T_{\text{eff}}, \log g, \xi$ )=(16375, 2.45, 7.5)

<sup>b</sup>( $T_{\text{eff}}, \log g, \xi$ )=(17000, 2.60, 7.5)

Table 2. Photospheric line by line NLTE and LTE abundances, and the line’s measured equivalent width ( $W_\lambda$ ) in mÅ for BD–9°4395

Line	$\chi$		$W_\lambda$ (mÅ)	$\log \epsilon(X)$	
	(eV)	$\log gf$		NLTE <sup>a</sup>	LTE <sup>b</sup>
H I $\lambda$ 3970.072	10.199	–0.993	60	9.16	8.90
H I $\lambda$ 4101.734	10.199	–0.753	65	9.12	8.72
H I $\lambda$ 4861.323	10.199	–0.020	200	9.10	8.75
Mean...	...	...	...	9.13±0.03	8.79±0.10
C II $\lambda$ 4313.106	23.116	–0.373	108	9.27	9.43
C II $\lambda$ 4325.832	23.119	–0.373			
C II $\lambda$ 4326.164	23.116	–0.407	131	9.04	9.17
C II $\lambda$ 4374.281	24.654	+0.660 <sup>c</sup>			
C II $\lambda$ 4375.008	24.658	–0.610 <sup>c</sup>	189	9.01	9.06
Mean...	...	...	...	9.11±0.14	9.22±0.19
C III $\lambda$ 4515.352	39.401	–0.756			
C III $\lambda$ 4515.811	39.402	–0.279	28	8.92	8.71
C III $\lambda$ 4647.418	29.535	+0.070	354	9.04	9.15
C III $\lambda$ 4651.473	29.535	–0.629	219	9.23	9.12
Mean...	...	...	...	9.06±0.16	8.99±0.25
N II $\lambda$ 4601.478	18.466	–0.428	125	7.66	7.98
N II $\lambda$ 4607.153	18.462	–0.507	103	7.60	7.93
N II $\lambda$ 4621.393	18.466	–0.514	98	7.57	7.91
N II $\lambda$ 4630.539	18.483	+0.094	224	7.70	7.98
Mean...	...	...	...	7.63±0.06	7.95±0.04
N III $\lambda$ 4103.390	27.438	–0.359	84	7.69	7.88
N III $\lambda$ 4195.740	36.842	–0.004	20	7.94	8.39
N III $\lambda$ 4200.070	36.856	+0.250	20	7.69	8.14
Mean...	...	...	...	7.77±0.14	8.14±0.26
O II $\lambda$ 4072.153	25.650	+0.552	134	8.13	7.78
O II $\lambda$ 4078.842	25.638	–0.284	32	7.99	7.77
O II $\lambda$ 4085.112	25.650	–0.189	46	8.10	7.86
O II $\lambda$ 4104.724	25.837	–0.302			
O II $\lambda$ 4104.990	25.837	–0.015	75	8.05	7.80
O II $\lambda$ 4303.833	28.822	+0.640 <sup>c</sup>	40	7.97	7.67
O II $\lambda$ 4331.857	28.512	–0.136	42	8.34	8.41
O II $\lambda$ 4336.859	22.979	–0.763	76	8.08	8.13
O II $\lambda$ 4342.009	28.883	+0.820 <sup>c</sup>	44	7.84	7.51
O II $\lambda$ 4345.560	22.979	–0.346	119	7.98	8.00
O II $\lambda$ 4349.426	22.999	+0.060	212	8.09	8.10
O II $\lambda$ 4351.457	25.661	–1.004			
O II $\lambda$ 4351.260	25.661	+0.227	92	8.13	7.83

Table 2—Continued

Line	$\chi$		$W_\lambda$ (mÅ)	log $\epsilon(X)$	
	(eV)	log $gf$		NLTE <sup>a</sup>	LTE <sup>b</sup>
O II $\lambda$ 4366.895	22.999	−0.348	134	8.08	8.09
O II $\lambda$ 4414.899	23.442	+0.172	206	7.86	8.06
O II $\lambda$ 4416.975	23.419	−0.077	162	7.91	8.07
O II $\lambda$ 4452.378	23.442	−0.788	56	7.92	8.09
O II $\lambda$ 4590.974	25.661	+0.350	132	8.38	8.01
O II $\lambda$ 4595.957	25.661	−1.033			
O II $\lambda$ 4596.177	25.661	+0.200	109	8.32	7.99
O II $\lambda$ 4609.373	29.069	+0.670 <sup>c</sup>	54	7.97	7.88
O II $\lambda$ 4661.632	22.979	−0.278	141	8.01	8.07
O II $\lambda$ 4705.346	26.249	+0.477	94	7.42	7.78
O II $\lambda$ 4941.072	26.554	−0.053	45	8.27	7.97
Mean...	...	...	...	8.04±0.21	7.95±0.20
Ne I $\lambda$ 5852.488	16.850	−0.490	21	8.20	8.65
Ne I $\lambda$ 6143.063	16.620	−0.100	63	8.18	8.77
Ne I $\lambda$ 6266.495	16.710	−0.370	42	8.11	8.85
Ne I $\lambda$ 6334.428	16.620	−0.320	36	8.13	8.71
Ne I $\lambda$ 6382.992	16.670	−0.240	48	8.17	8.79
Ne I $\lambda$ 6402.246	16.620	+0.330	143	8.19	8.89
Ne I $\lambda$ 6506.528	16.670	−0.030	65	8.13	8.75
Ne I $\lambda$ 6598.953	16.850	−0.360	34	8.39	8.79
Ne I $\lambda$ 7032.413	16.620	−0.260	46	8.16	8.80
Mean...	...	...	...	8.18±0.08	8.78±0.07
Ne II $\lambda$ 4379.552	34.802	+0.780	38	8.05	8.04
Ne II $\lambda$ 4413.113	34.833	+0.520	22	8.02	8.01
Mean...	...	...	...	8.04±0.02	8.03±0.02

<sup>a</sup>( $T_{\text{eff}}, \log g, \xi$ )=(24300, 2.65, 17.5)

<sup>b</sup>( $T_{\text{eff}}, \log g, \xi$ )=(24800, 2.85, 23.0)

<sup>c</sup>Wiese, Smith, & Glennon (1966)

Table 3. Photospheric line by line LTE neon abundances, NLTE neon abundance, and the line’s measured equivalent width ( $W_\lambda$ ) in mÅ for LSE 78

Line	$\chi$		$W_\lambda$ (mÅ)	$\log \epsilon(\text{Ne})$	
	(eV)	$\log gf$		NLTE <sup>b</sup>	LTE <sup>a</sup>
Ne I $\lambda$ 5852.488	16.850	-0.490	155		9.36
Ne I $\lambda$ 5881.895	16.620	-0.770	128		9.46
Ne I $\lambda$ 6029.997	16.670	-1.040	81		9.49
Ne I $\lambda$ 6074.338	16.670	-0.500	159		9.37
Ne I $\lambda$ 6143.063	16.620	-0.100	285		9.52
Ne I $\lambda$ 6163.594	16.710	-0.620	137		9.40
Ne I $\lambda$ 6217.281	16.620	-0.960	84		9.42
Ne I $\lambda$ 6266.495	16.710	-0.370	222		9.55
Ne I $\lambda$ 6334.428	16.620	-0.320	241		9.57
Ne I $\lambda$ 6382.992	16.670	-0.240	254		9.56
Ne I $\lambda$ 6402.246	16.620	+0.330	409		9.59
Ne I $\lambda$ 6506.528	16.670	-0.030	287		9.49
Ne I $\lambda$ 6532.882	16.710	-0.720	123		9.47
Ne I $\lambda$ 6598.953	16.850	-0.360	119		9.11
Ne I $\lambda$ 6717.043	16.850	-0.360	138		9.22
Ne I $\lambda$ 7032.413	16.620	-0.260	229		9.47
Mean...	...	...	...	8.67	9.40±0.13

<sup>a</sup>( $T_{\text{eff}}, \log g, \xi$ )=(18300, 2.20, 16.0)

<sup>b</sup>By applying correction on the LTE neon abundance

Table 4. Photospheric line by line LTE neon abundances, NLTE neon abundance, and the line’s measured equivalent width ( $W_\lambda$ ) in mÅ for V1920,Cyg

Line	$\chi$		$W_\lambda$ (mÅ)	$\log \epsilon(\text{Ne})$	
	(eV)	$\log gf$		NLTE <sup>b</sup>	LTE <sup>a</sup>
Ne I $\lambda$ 5852.488	16.850	-0.490	185		9.18
Ne I $\lambda$ 5881.895	16.620	-0.770	204		9.47
Ne I $\lambda$ 6029.997	16.670	-1.040	114		9.38
Ne I $\lambda$ 6074.338	16.670	-0.500	230		9.34
Ne I $\lambda$ 6143.063	16.620	-0.100	359		9.44
Ne I $\lambda$ 6163.594	16.710	-0.620	198		9.35
Ne I $\lambda$ 6217.281	16.620	-0.960	93		9.18
Ne I $\lambda$ 6266.495	16.710	-0.370	264		9.38
Ne I $\lambda$ 6334.428	16.620	-0.320	258		9.28
Ne I $\lambda$ 6382.992	16.670	-0.240	319		9.45
Ne I $\lambda$ 6402.246	16.620	+0.330	472		9.47
Ne I $\lambda$ 6506.528	16.670	-0.030	373		9.46
Ne I $\lambda$ 6532.882	16.710	-0.720	176		9.40
Ne I $\lambda$ 6598.953	16.850	-0.360	177		9.07
Ne I $\lambda$ 6717.043	16.850	-0.360	177		9.09
Ne I $\lambda$ 7032.413	16.620	-0.260	340		9.55
Mean...	...	...	...	8.50	9.30±0.14

<sup>a</sup>( $T_{\text{eff}}, \log g, \xi$ )=(16330, 1.80, 20.0)

<sup>b</sup>By applying correction on the LTE neon abundance

Table 5. Photospheric line by line LTE neon abundances, NLTE neon abundance, and the line’s measured equivalent width ( $W_\lambda$ ) in mÅ for HD 124448

Line	$\chi$		$W_\lambda$ (mÅ)	$\log \epsilon(\text{Ne})$	
	(eV)	$\log gf$		NLTE <sup>b</sup>	LTE <sup>a</sup>
Ne I $\lambda$ 6334.428	16.620	-0.320	118		8.45
Ne I $\lambda$ 6717.043	16.850	-0.360	105		8.51
Mean...	...	...	...	7.70	8.50±0.04

<sup>a</sup>( $T_{\text{eff}}, \log g, \xi$ )=(15500, 1.90, 12.0)

<sup>b</sup>By applying correction on the LTE neon abundance

Table 6. Photospheric line by line LTE neon abundances, NLTE neon abundance, and the line’s measured equivalent width ( $W_\lambda$ ) in mÅ for PV Tel

Line	$\chi$		$W_\lambda$ (mÅ)	log $\epsilon(\text{Ne})$	
	(eV)	log $gf$		NLTE <sup>b</sup>	LTE <sup>a</sup>
Ne I $\lambda$ 5881.895	16.620	−0.770	233		8.52
Ne I $\lambda$ 6074.338	16.670	−0.500	324		8.53
Ne I $\lambda$ 6096.163	16.670	−0.310	354		8.42
Ne I $\lambda$ 6402.246	16.620	+0.330	671		8.70
Ne I $\lambda$ 7032.413	16.620	−0.260	422		8.58
Mean...	...	...	...	7.60	8.53±0.08

<sup>a</sup>( $T_{\text{eff}}, \log g, \xi$ )=(13750, 1.60, 25.0)

<sup>b</sup>By applying correction on the LTE neon abundance

Table 7. Photospheric line by line NLTE and LTE abundances, and the line’s measured equivalent width ( $W_\lambda$ ) in mÅ for LSIV +6° 002

Line	$\chi$		$W_\lambda$ (mÅ)	$\log \epsilon(X)$	
	(eV)	$\log gf$		NLTE <sup>a</sup>	LTE <sup>b</sup>
H I $\lambda$ 4340.462	10.199	−0.447	20	8.15	7.95
H I $\lambda$ 4861.323	10.199	−0.020	11	7.80	7.34
Mean...	...	...	...	7.98±0.25	7.65±0.43
C II $\lambda$ 4267.001	18.046	+0.563			
C II $\lambda$ 4267.183	18.046	+0.716			
C II $\lambda$ 4267.261	18.046	−0.584	331	8.70?	8.90?
C II $\lambda$ 4285.703	24.602	−0.430 <sup>c</sup>	61	9.42	9.57
C II $\lambda$ 4291.815	24.603	−0.500 <sup>d</sup>			
C II $\lambda$ 4291.858	24.603	−0.500 <sup>d</sup>	107	9.67	10.18?
C II $\lambda$ 4313.106	23.116	−0.373	85	9.31	9.50
C II $\lambda$ 4317.265	23.119	−0.005	147	9.53	9.72
C II $\lambda$ 4318.606	23.114	−0.407	64	9.12	9.30
C II $\lambda$ 4372.375	24.656	+0.057 <sup>c</sup>	162	9.96?	10.12?
C II $\lambda$ 4413.271	24.603	−0.610	67	9.70	9.85
Mean...	...	...	...	9.46±0.22	9.59±0.21
C III $\lambda$ 4067.940	39.923	+0.720	154	9.25	8.85
C III $\lambda$ 4068.916	39.924	+0.838			
C III $\lambda$ 4068.916	39.924	−0.340	155	9.11	8.71
C III $\lambda$ 4070.260	39.925	+0.953			
C III $\lambda$ 4070.306	39.925	−0.339	170	9.10	8.70
C III $\lambda$ 4186.900	40.010	+0.918	181	9.29	8.88
C III $\lambda$ 4647.418	29.535	+0.070	299	9.24	9.08
C III $\lambda$ 4650.246	29.535	−0.151	262	9.30	9.10
C III $\lambda$ 4651.473	29.535	−0.629	168	9.21	8.85
C III $\lambda$ 4659.058	38.218	−0.654	59	9.60	9.18
C III $\lambda$ 4663.642	38.219	−0.530	63	9.53	9.12
C III $\lambda$ 4665.860	38.226	+0.044	101	9.40	9.01
C III $\lambda$ 4673.953	38.226	−0.433	69	9.52	9.11
Mean...	...	...	...	9.32±0.17	8.96±0.17
N II $\lambda$ 3994.997	18.497	+0.208	139	7.88	8.34
N II $\lambda$ 4035.081	23.124	+0.623 <sup>e</sup>	97	8.01	8.27



Table 7—Continued

Line	$\chi$		$W_\lambda$ (mÅ)	$\log \epsilon(X)$	
	(eV)	$\log gf$		NLTE <sup>a</sup>	LTE <sup>b</sup>
N II $\lambda$ 4041.310	23.142	+0.853 <sup>e</sup>	129	8.10	8.37
N II $\lambda$ 4043.532	23.132	+0.743 <sup>e</sup>	92	7.84	8.10
N II $\lambda$ 4044.779	23.132	−0.437 <sup>e</sup>	66	8.74	8.99
N II $\lambda$ 4056.907	23.142	−0.437 <sup>e</sup>	49	8.53	8.78
N II $\lambda$ 4073.053	23.124	−0.160 <sup>d</sup>	62	8.42	8.67
N II $\lambda$ 4082.270	23.132	+0.150 <sup>d</sup>	70	8.21	8.46
N II $\lambda$ 4173.561	23.242	−0.570 <sup>d</sup>	42	8.60	8.85
N II $\lambda$ 4179.674	23.246	−0.090 <sup>d</sup>	55	8.30	8.55
N II $\lambda$ 4236.927	23.239	+0.383 <sup>e</sup>			
N II $\lambda$ 4237.047	23.242	+0.553 <sup>d</sup>	109	7.93	8.18
N II $\lambda$ 4427.233	23.422	−0.010 <sup>d</sup>	58	8.33	8.57
N II $\lambda$ 4427.963	23.422	−0.170 <sup>e</sup>	60	8.50	8.74
N II $\lambda$ 4431.814	23.415	−0.170 <sup>e</sup>	47	8.33	8.57
N II $\lambda$ 4432.736	23.415	+0.580 <sup>e</sup>	92	8.09	8.34
N II $\lambda$ 4433.475	23.425	−0.040 <sup>e</sup>	58	8.35	8.58
N II $\lambda$ 4442.015	23.422	+0.310 <sup>e</sup>	50	7.89	8.13
N II $\lambda$ 4447.030	20.409	+0.228	110	8.03	8.40
N II $\lambda$ 4530.410	23.475	+0.670 <sup>e</sup>	103	8.16	8.41
N II $\lambda$ 4601.478	18.466	−0.428	112	8.30	8.74
N II $\lambda$ 4607.153	18.462	−0.507	118	8.45	8.89
N II $\lambda$ 4613.868	18.466	−0.665	93	8.34	8.76
N II $\lambda$ 4621.393	18.466	−0.514	122	8.50	8.94
N II $\lambda$ 4630.539	18.483	+0.094	173	8.45	8.97
N II $\lambda$ 4678.135	23.572	+0.434 <sup>e</sup>	66	8.04	8.27
N II $\lambda$ 4694.642	23.572	+0.100 <sup>d</sup>	65	8.37	8.61
N II $\lambda$ 4774.244	20.646	−1.257	27	8.55	8.87
N II $\lambda$ 4779.722	20.646	−0.587	58	8.35	8.68
N II $\lambda$ 4781.190	20.654	−1.308	19	8.43	8.74
N II $\lambda$ 4793.648	20.654	−1.095	33	8.51	8.83
N II $\lambda$ 4803.287	20.666	−0.113	88	8.23	8.57
N II $\lambda$ 4810.299	20.666	−1.084	26	8.37	8.68
Mean...	...	...	...	8.29±0.23	8.59±0.25
N III $\lambda$ 4097.360	27.438	−0.057	184	8.23	8.39
N III $\lambda$ 4103.390	27.438	−0.359	169	8.44	8.56
N III $\lambda$ 4215.770	36.856	−0.705	18	8.41	8.54
N III $\lambda$ 4379.201	39.711	+1.010 <sup>c</sup>	133	8.31	8.90
N III $\lambda$ 4514.850	35.671	+0.221	112	9.15?	9.10?
N III $\lambda$ 4518.140	35.649	−0.461	75	9.40?	9.33?
N III $\lambda$ 4523.560	35.657	−0.353	51	8.91?	8.86
N III $\lambda$ 4527.860	38.958	−0.471 <sup>c</sup>	23	8.41	8.88

Table 7—Continued

Line	$\chi$		$W_\lambda$ (mÅ)	$\log \epsilon(X)$	
	(eV)	$\log gf$		NLTE <sup>a</sup>	LTE <sup>b</sup>
N III $\lambda$ 4535.050	38.958	−0.170 <sup>c</sup>	26	8.19	8.66
N III $\lambda$ 4539.700	38.645	−0.452	33	8.64	9.07?
N III $\lambda$ 4544.840	39.396	−0.151	33	8.34	8.77
N III $\lambda$ 4546.330	38.958	+0.004 <sup>c</sup>	21	7.90	8.35
N III $\lambda$ 4634.130	30.459	−0.086	115	8.63	8.47
N III $\lambda$ 4640.640	30.463	+0.168	131	8.50	8.37
N III $\lambda$ 4641.850	30.463	−0.788	139	9.53?	9.41?
Mean...	...	...	...	8.36±0.21	8.61±0.21
O II $\lambda$ 4069.623	25.631	+0.150			
O II $\lambda$ 4069.882	25.638	+0.344	140	8.25	8.18
O II $\lambda$ 4072.153	25.650	+0.552	88	8.04	7.96
O II $\lambda$ 4085.112	25.650	−0.189	49	8.68	8.22
O II $\lambda$ 4092.929	25.665	−0.308	38	8.40	8.18
O II $\lambda$ 4366.895	22.999	−0.348	115	8.39	8.72
O II $\lambda$ 4414.899	23.442	+0.172	118	7.93	8.30
O II $\lambda$ 4416.975	23.419	−0.077	134	8.31	8.73
O II $\lambda$ 4452.378	23.442	−0.788	55	8.25	8.53
O II $\lambda$ 4590.974	25.661	+0.350	99	8.43	8.36
O II $\lambda$ 4595.957	25.661	−1.033			
O II $\lambda$ 4596.177	25.661	+0.200	87	8.38	8.30
O II $\lambda$ 4638.856	22.966	−0.332	110	8.34	8.67
O II $\lambda$ 4649.135	22.999	+0.308	151	8.08	8.52
O II $\lambda$ 4661.632	22.979	−0.278	90	8.09	8.39
O II $\lambda$ 4676.235	22.999	−0.394	67	7.95	8.23
O II $\lambda$ 4696.353	28.510	−1.380	16	8.07	8.36
Mean...	...	...	...	8.24±0.20	8.38±0.22
Ne II $\lambda$ 4217.169	34.609	+0.090 <sup>d</sup>	45	8.59	8.57
Ne II $\lambda$ 4219.745	34.609	+0.750 <sup>d</sup>	99	8.60	8.64
Ne II $\lambda$ 4220.894	34.619	−0.060 <sup>d</sup>			
Ne II $\lambda$ 4221.087	34.619	−0.740 <sup>d</sup>	37	8.52	8.49
Ne II $\lambda$ 4224.472	34.632	−0.860 <sup>d</sup>			
Ne II $\lambda$ 4224.642	34.632	−0.750 <sup>d</sup>	23	8.77	8.75
Ne II $\lambda$ 4231.532	34.619	−0.080 <sup>d</sup>			
Ne II $\lambda$ 4231.636	34.619	+0.260 <sup>d</sup>	60	8.46	8.44

Table 7—Continued

Line	$\chi$		$W_\lambda$ (mÅ)	log $\epsilon(X)$	
	(eV)	log $gf$		NLTE <sup>a</sup>	LTE <sup>b</sup>
Ne II $\lambda$ 4239.911	34.632	-0.490 <sup>d</sup>			
Ne II $\lambda$ 4240.105	34.632	-0.020 <sup>d</sup>	50	8.62	8.59
Ne II $\lambda$ 4250.645	34.632	+0.150 <sup>d</sup>	46	8.58	8.56
Ne II $\lambda$ 4397.991	34.814	+0.160 <sup>d</sup>	61	8.91	8.82
Ne II $\lambda$ 4430.946	34.749	+0.310 <sup>d</sup>	72	8.78	8.81
Mean...	...	...	...	8.65±0.14	8.63±0.14

<sup>a</sup>( $T_{\text{eff}}, \log g, \xi$ )=(30000, 4.10, 9.0)

<sup>b</sup>( $T_{\text{eff}}, \log g, \xi$ )=(32000, 4.20, 9.0)

<sup>c</sup>Jeffery (1998)

<sup>d</sup>Kurucz  $gf$ -value

<sup>e</sup>Wiese, Smith, & Glennon (1966)

Table 8. He, C, N, O, Ne, and Fe abundances of the sample EHe stars

Star	$(T_{\text{eff}}, \log g)$	log $\epsilon(X)$					Fe <sup>a</sup>
		He	C	N	O	Ne	
LSIV +6° 002	(30000, 4.10)	11.54	9.4	8.3	8.2	8.65	7.1
BD-9° 4395	(24300, 2.65)	11.54	9.1	7.8	8.0	8.18	6.6
LSE 78	(18300, 2.20)	11.54	9.4	8.3	9.4	8.67	6.8
BD+10° 2179	(16375, 2.45)	11.54	9.3	8.1	7.9	7.87	6.2
V1920 Cyg	(16330, 1.80)	11.50	9.6	8.6	9.9	8.50	6.8
HD 124448	(15500, 1.90)	11.54	9.1	8.7	8.3	7.70	7.2
PV Tel	(13750, 1.60)	11.54	9.2	8.7	8.8	7.60	7.0

<sup>a</sup>LTE abundance

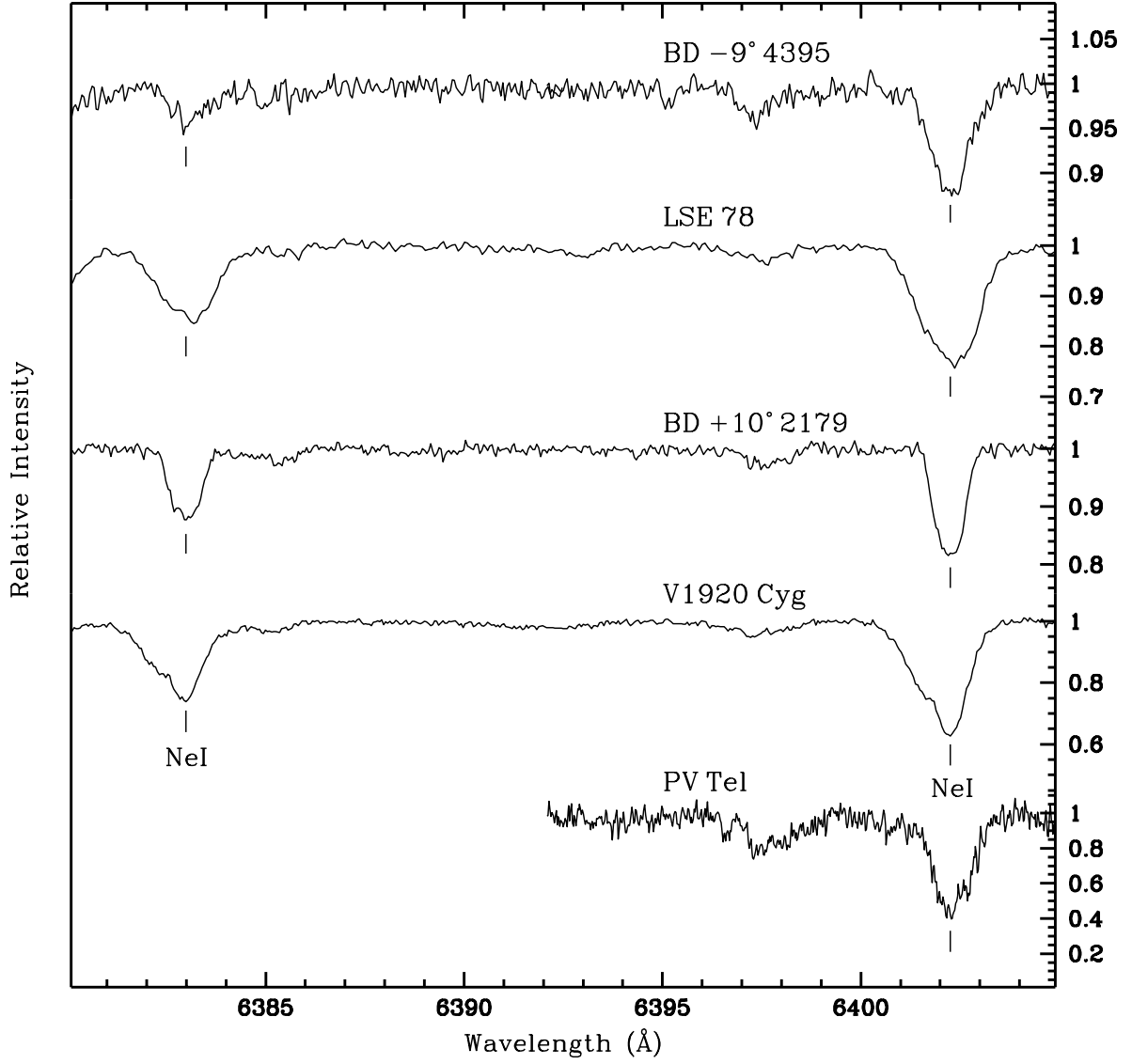


Fig. 1.— The spectral region from 6380 – 6405 Å is shown for five EHe stars with the hottest star at the top and the coolest star at the bottom. The NeI lines at 6382.99 Å and at 6402.25 Å are marked.

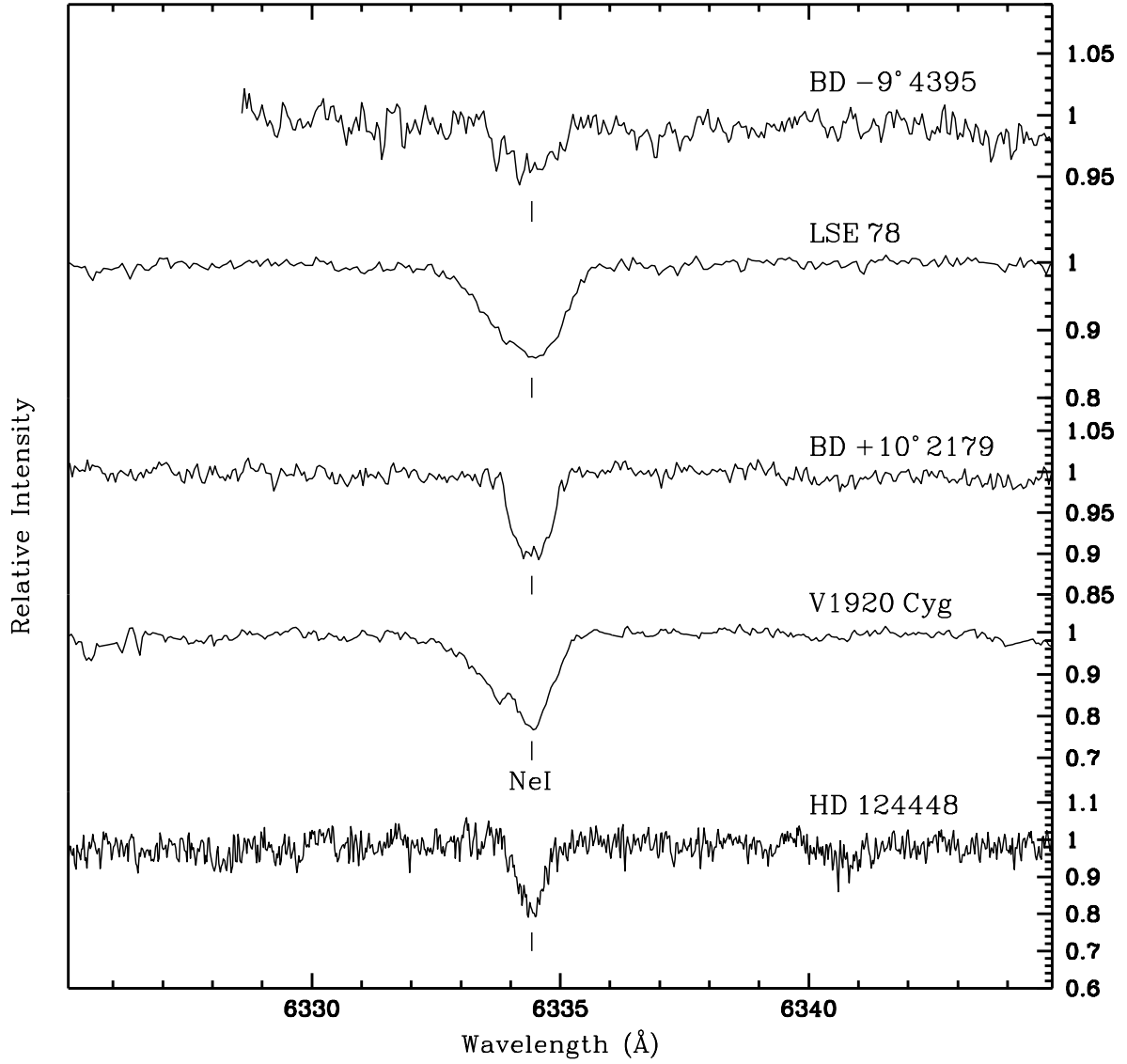


Fig. 2.— The spectral region from 6325 – 6345 Å is shown for five EHe stars with the hottest star at the top and the coolest star at the bottom. The Ne I line at 6334.43 Å is marked.

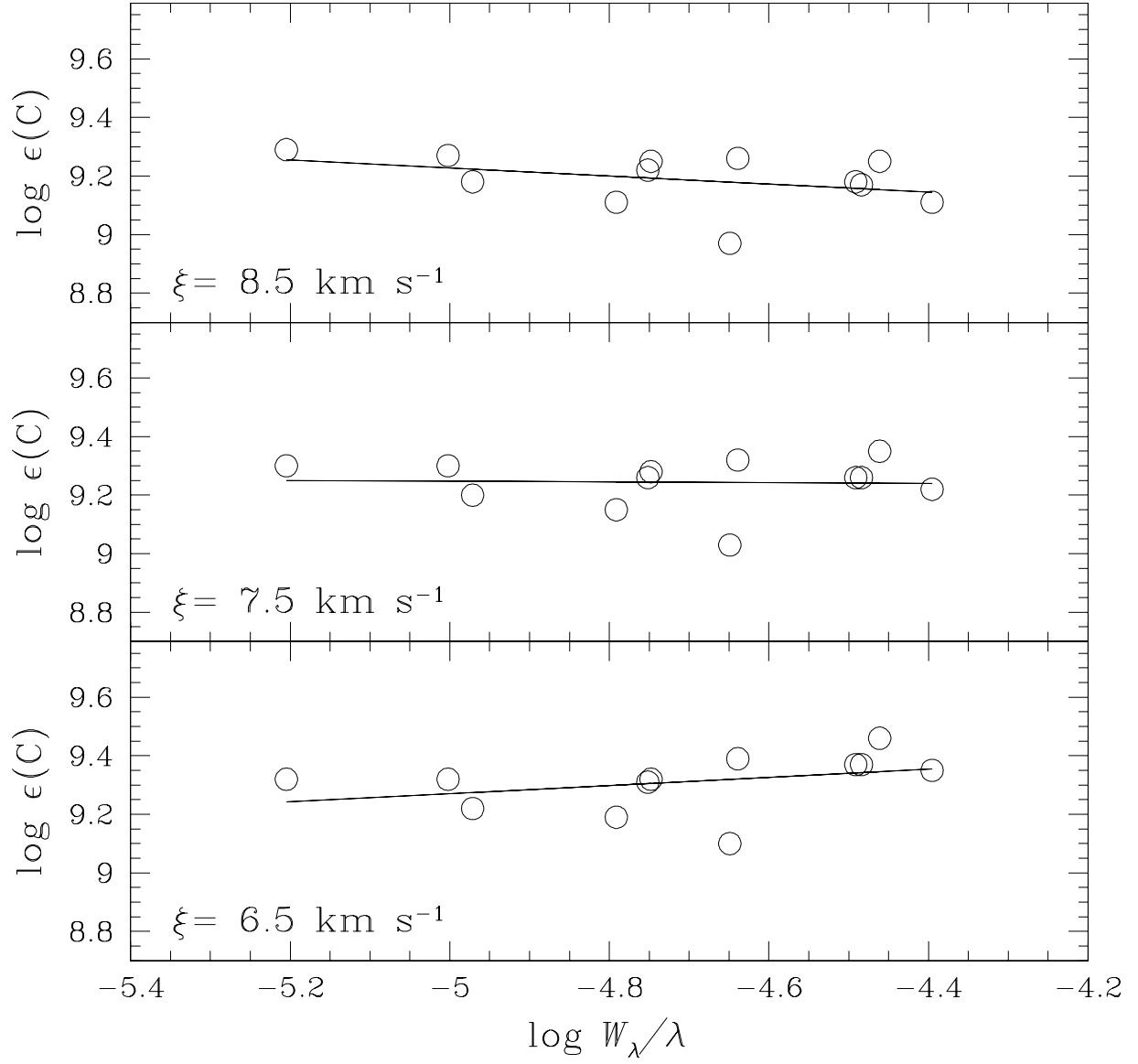


Fig. 3.— NLTE abundances from C II lines for BD +10° 2179 versus their reduced equivalent widths ( $\log W_\lambda/\lambda$ ). A microturbulent velocity of  $\xi = 7.5 \text{ km s}^{-1}$  is obtained from this figure.

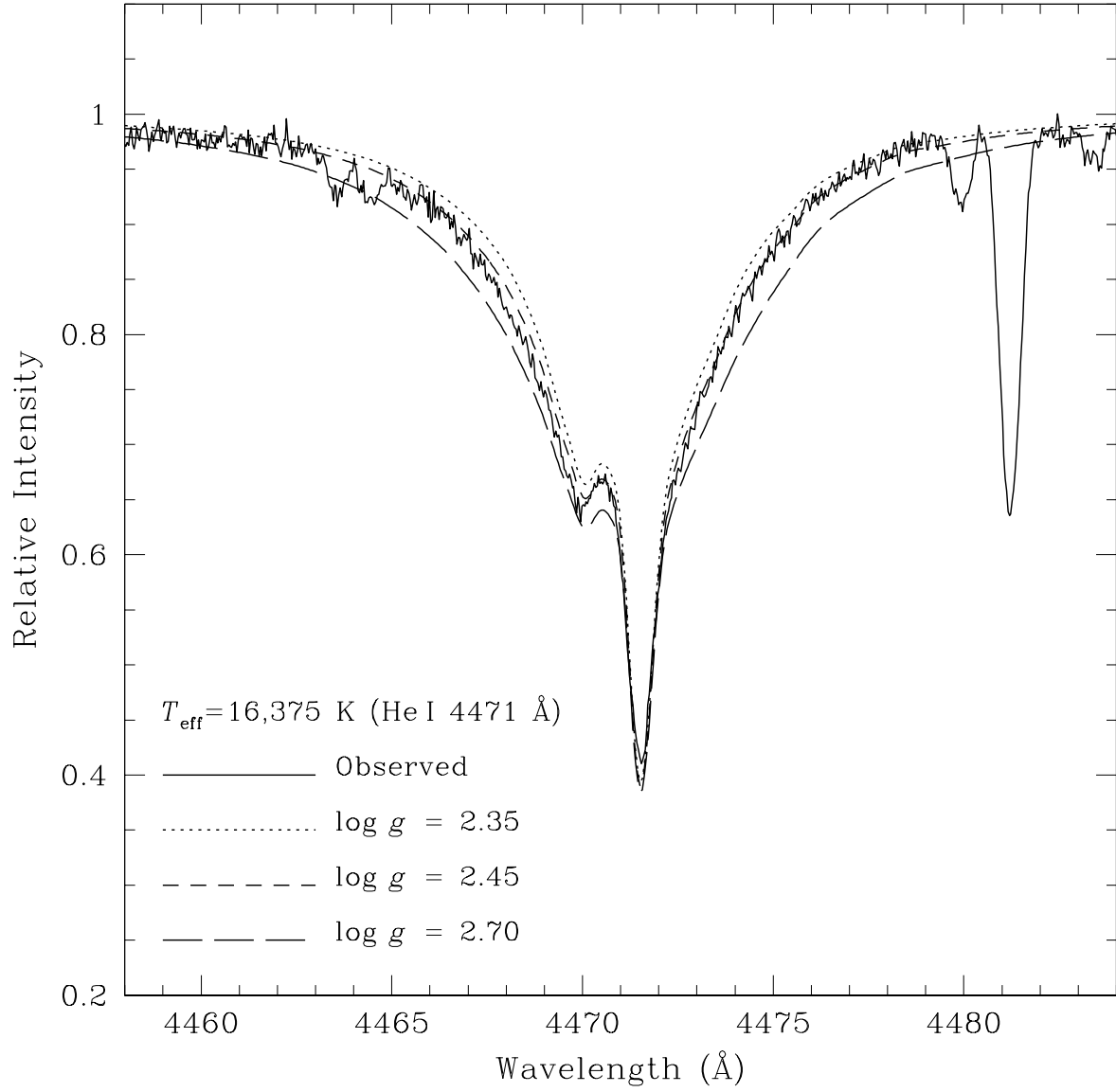


Fig. 4.— BD+10° 2179’s observed and synthesized NLTE He I line profile at 4471  $\text{\AA}$ . The NLTE He I line profiles are synthesized using the NLTE model  $T_{\text{eff}}=16,375$  K, for three different  $\log g$  values – see key on the figure.

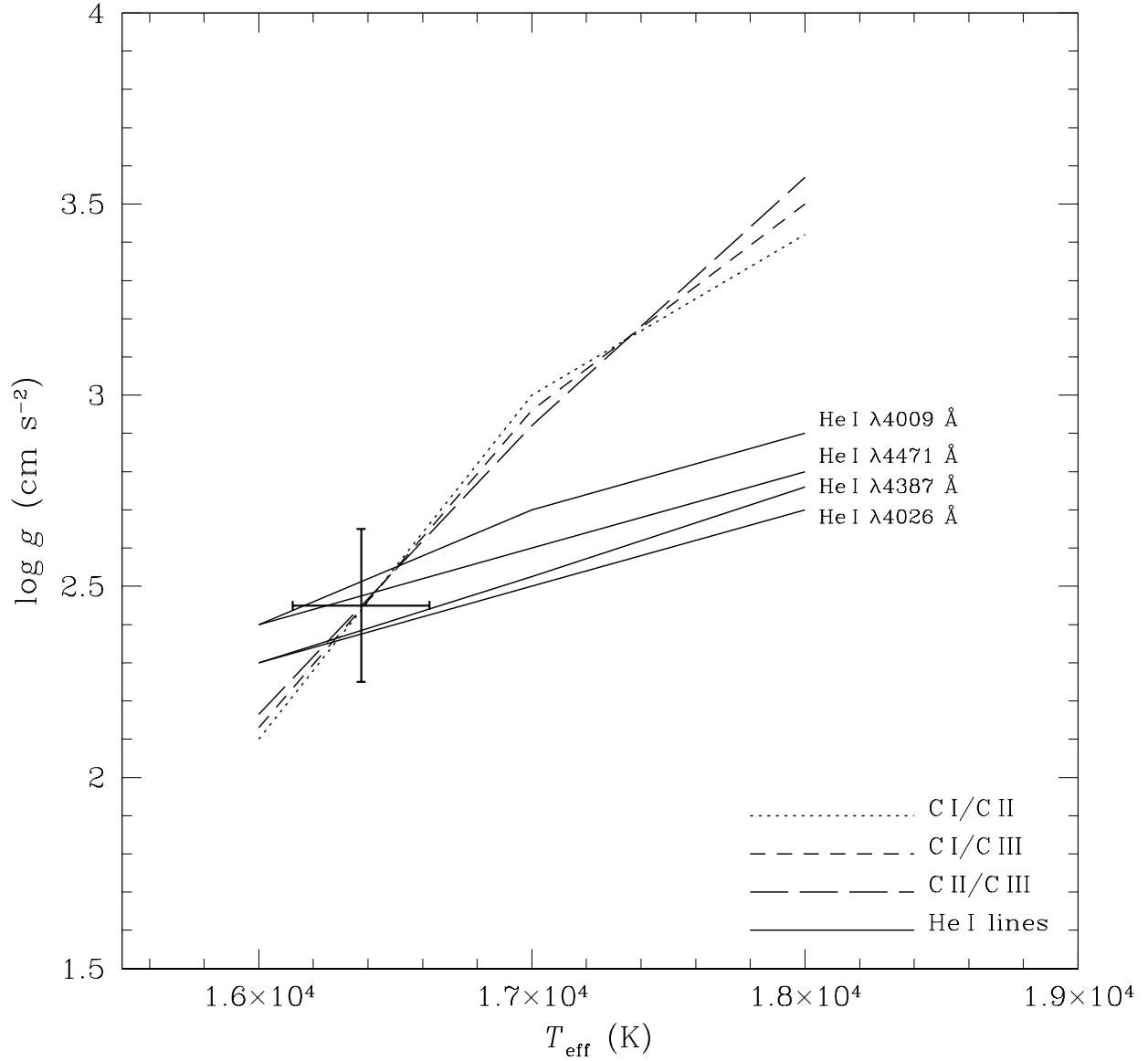


Fig. 5.— The  $T_{\text{eff}}$  vs  $\log g$  plane for BD +10° 2179. Loci satisfying ionization equilibria are plotted – see keys on the figure. The loci satisfying optical He I line profiles ( $\lambda$  4471, 4387, 4026, and 4009 Å) are shown by the solid lines. The cross shows the adopted NLTE model atmosphere parameters.



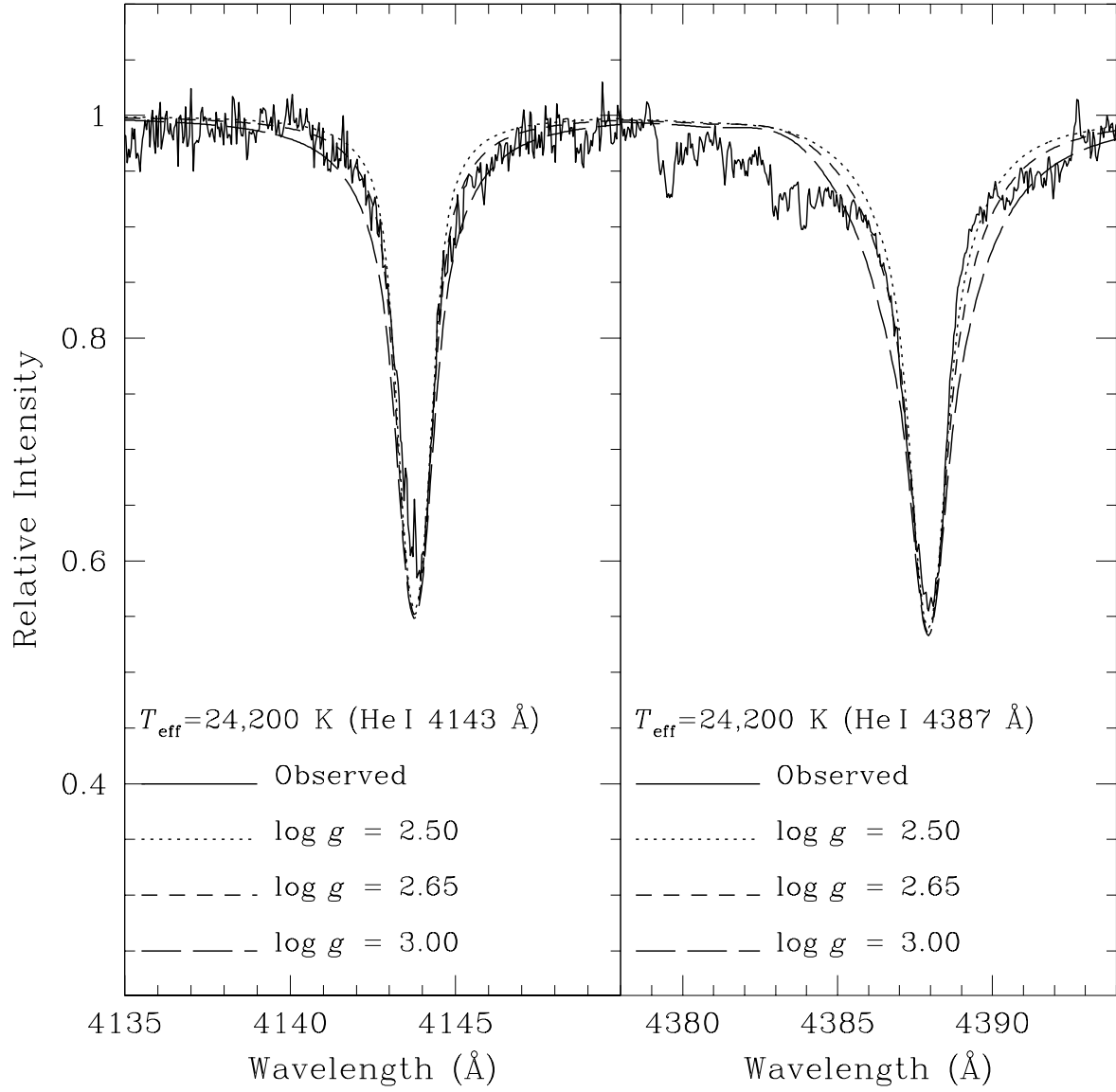


Fig. 6.— BD-9° 4395’s observed and synthesized NLTE He I line profiles at 4143 Å and at 4387 Å. The NLTE He I line profiles are synthesized using the NLTE model  $T_{\text{eff}} = 24,200$  K, for three different  $\log g$  values – see key on the figure.

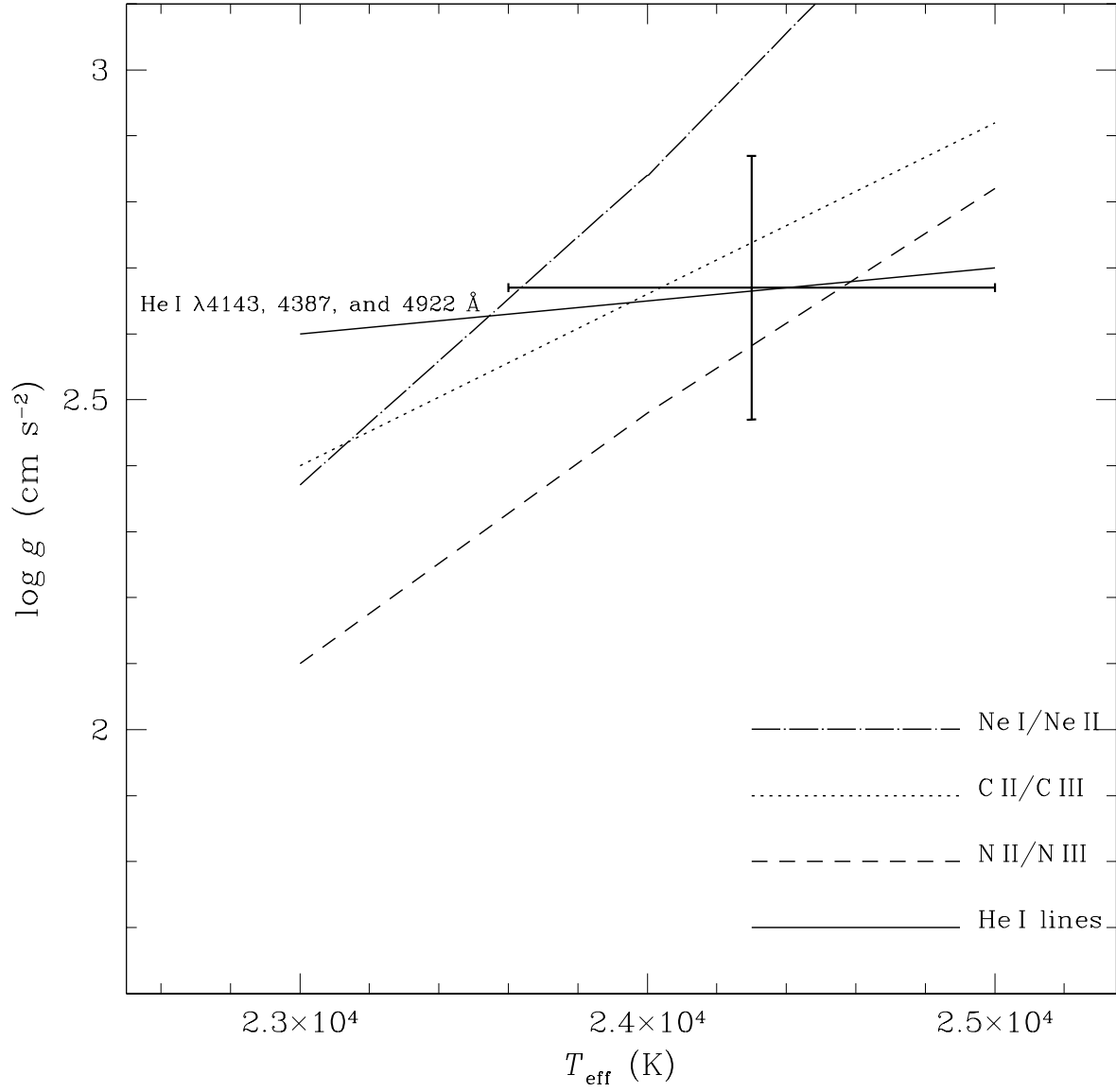


Fig. 7.— The  $T_{\text{eff}}$  vs  $\log g$  plane for BD-9° 4395. Loci satisfying ionization equilibria are plotted — see keys on the figure. The locus satisfying optical He I line profiles ( $\lambda$  4143, 4387, and 4922  $\text{\AA}$ ) is shown by the solid line. The cross shows the adopted NLTE model atmosphere parameters.

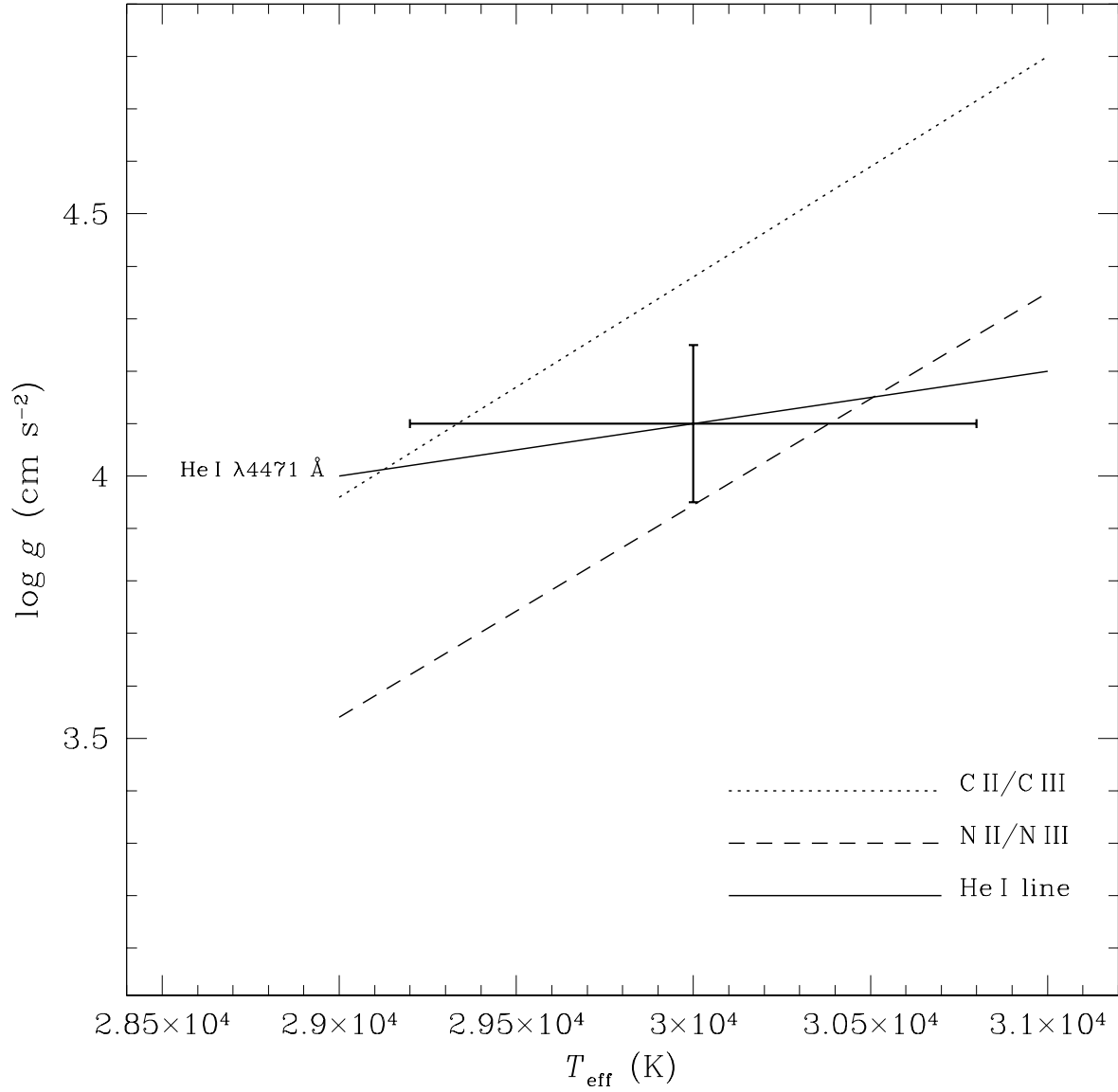


Fig. 8.— The  $T_{\text{eff}}$  vs  $\log g$  plane for LSIV +6° 002. Loci satisfying ionization equilibria are plotted – see keys on the figure. The locus satisfying optical He I 4471 Å line profile is shown by the solid line. The cross shows the adopted NLTE model atmosphere parameters.

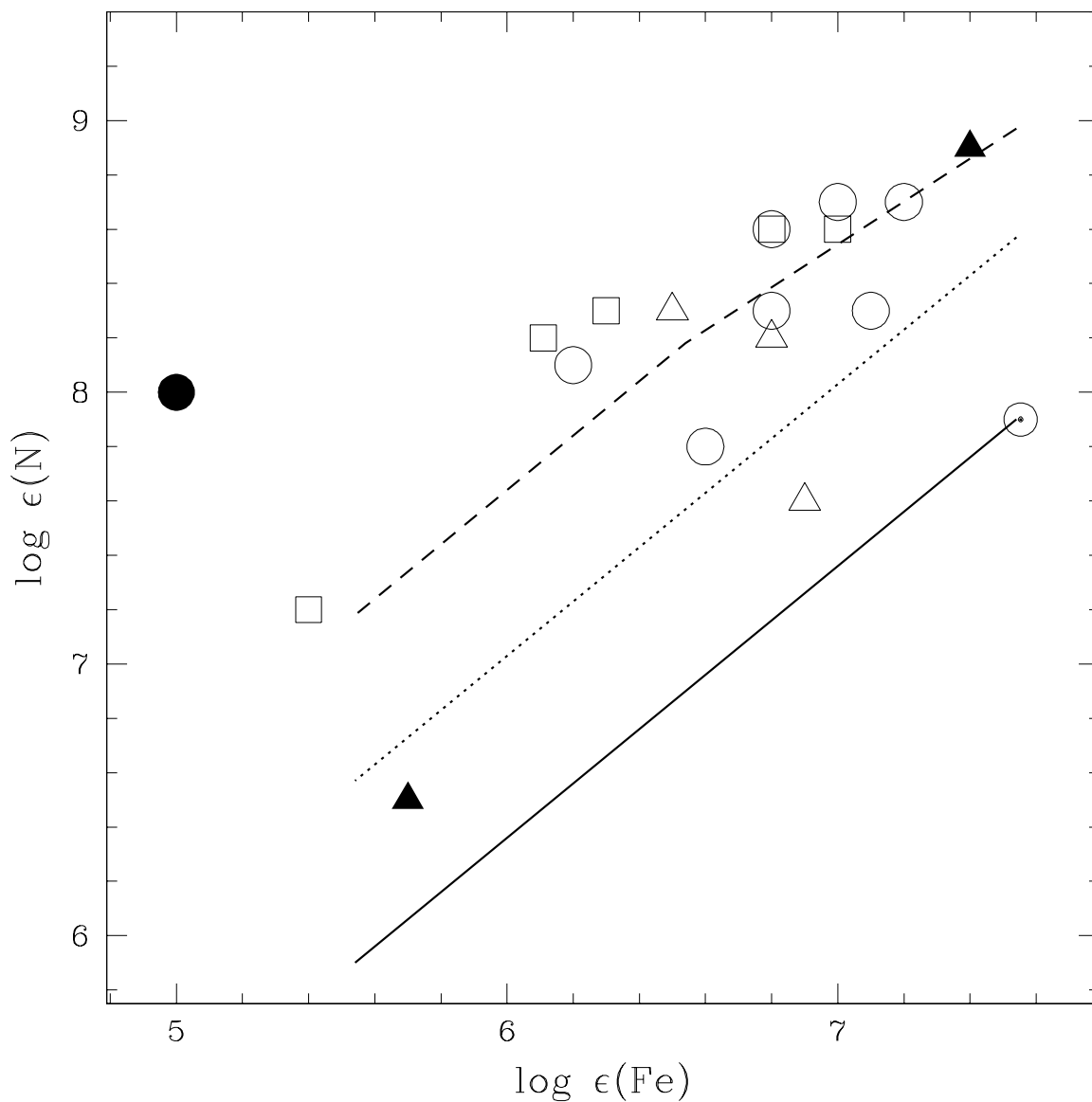


Fig. 9.— N vs. Fe. Our sample of seven EHes is represented by open circles. Five cool EHes are represented by open squares (Pandey et al. 2006; Pandey & Reddy 2006; Pandey et al. 2001). The results taken from the literature for EHes with C/He of about 1% (Drilling, Jeffery, & Heber 1998; Jeffery et al. 1998) are represented by open triangles. The two EHes of much lower C/He – V652 Her and HD 144941 – are shown by filled triangles (Jeffery & Harrison 1997; Harrison & Jeffery 1997; Jeffery, Hill & Heber 1999). DY Cen (Jeffery & Heber 1993) is represented by a filled circle. Circled dot represents the Sun.  $N = Fe$  is denoted by the solid line. The dotted line represents conversion of the initial sum of C and N to N. The dashed line represents the locus of the sum of initial C, N, and O converted to N.

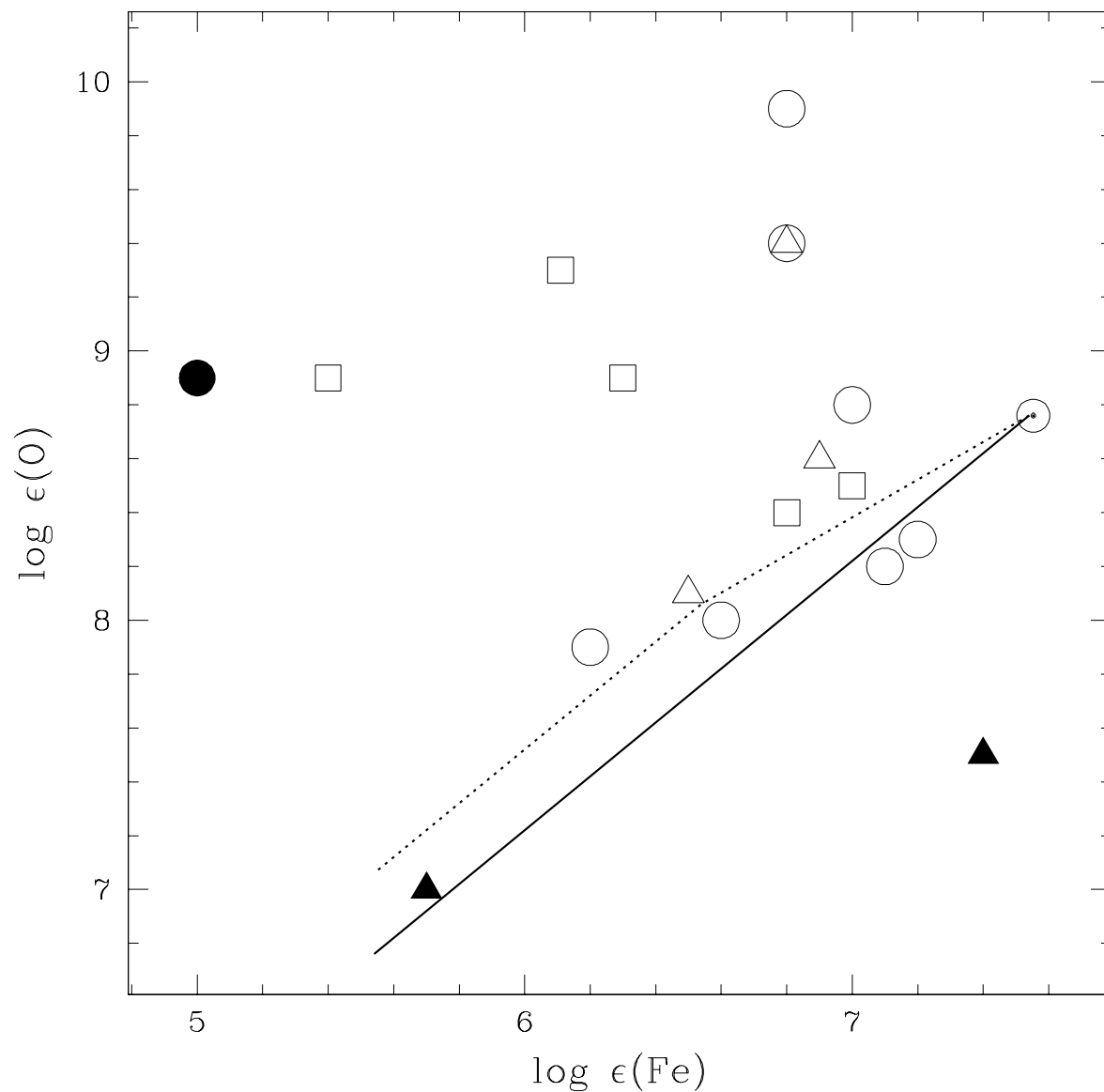


Fig. 10.— O vs. Fe. Our sample of seven EHes is represented by open circles. Five cool EHes are represented by open squares (Pandey et al. 2006; Pandey & Reddy 2006; Pandey et al. 2001). The results taken from the literature for EHes with C/He of about 1% (Drilling, Jeffery, & Heber 1998; Jeffery et al. 1998) are represented by open triangles. The two EHes of much lower C/He – V652 Her and HD 144941 – are shown by filled triangles (Jeffery & Harrison 1997; Harrison & Jeffery 1997; Jeffery, Hill & Heber 1999). DY Cen (Jeffery & Heber 1993) is represented by a filled circle. Circled dot represents the Sun.  $O = Fe$  is denoted by the solid line. The dotted line is from the relation  $[\alpha/Fe]$  vs.  $[Fe/H]$  for normal disk and halo stars (Ryde & Lambert 2004).

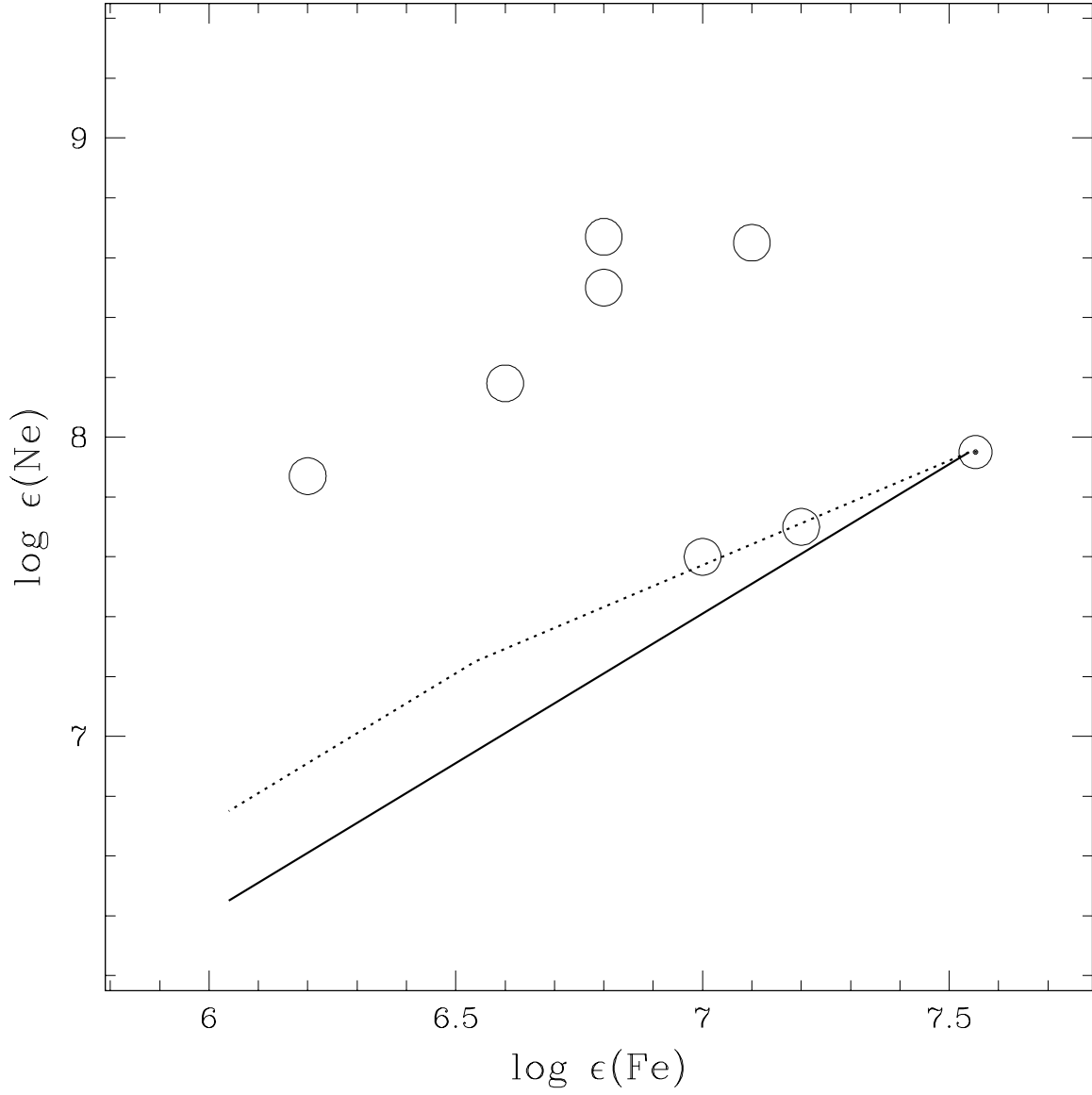


Fig. 11.— Ne vs. Fe. Our sample of seven EHe stars is represented by circles. The symbol  $\odot$  is the Sun. Ne = Fe is denoted by the solid line. The dotted line is from the relation  $[\alpha/\text{Fe}]$  vs.  $[\text{Fe}/\text{H}]$  for normal disk and halo stars (Ryde & Lambert 2004).

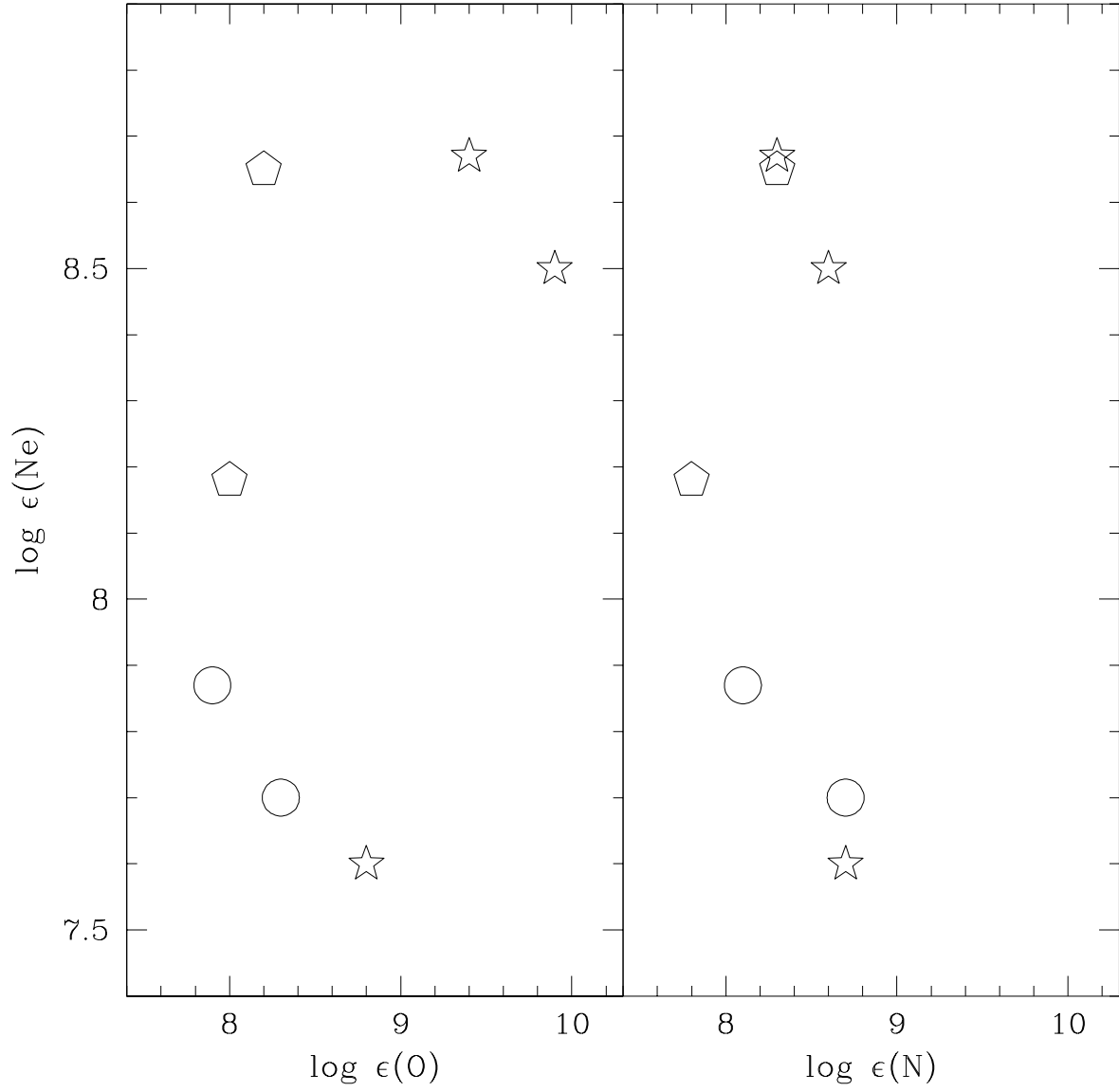


Fig. 12.— *Left*: Ne vs. O. Our sample of seven EHe stars. *s*-process enriched EHes are represented by stars. EHes with no *s*-process enrichment are represented by circles. EHes with no information on *s*-process enrichment are represented by pentagons. *Right*: Ne vs. N. The symbols have the same meaning as in the left panel.